Naval Research Laboratory

Washington, DC 20375-5320

NRL/MR/7130--06-8989

Hybrid Actuator for 3-Axis Control

PETER C. HERDIC

SFA, Inc.
Crofton, MD

ROBERT D. CORSARO
BRIAN H. HOUSTON

Physical Acoustics Branch
Acoustics Division

September 15, 2006

REPORT DOCUMENTATION PAGE

Form Approved
OMB No. 0704-0188

1. REPORT DATE *(DD-MM-YYYY)*	**2. REPORT TYPE**	**3. DATES COVERED** *(From - To)*
15-09-2006	Memorandum Report	

4. TITLE AND SUBTITLE

Hybrid Actuator for 3-Axis Control

5a. CONTRACT NUMBER

5b. GRANT NUMBER

5c. PROGRAM ELEMENT NUMBER

6. AUTHOR(S)

Peter C. Herdic,* Robert D. Corsaro, and Brian H. Houston

5d. PROJECT NUMBER

5e. TASK NUMBER

5f. WORK UNIT NUMBER

7. PERFORMING ORGANIZATION NAME(S) AND ADDRESS(ES)

Naval Research Laboratory
4555 Overlook Avenue, SW
Washington, DC 20375-5320

8. PERFORMING ORGANIZATION REPORT NUMBER

NRL/MR/7130--06-8989

9. SPONSORING / MONITORING AGENCY NAME(S) AND ADDRESS(ES)

KAPL, Inc.
Knolls Atomic Power Laboratory
P.O. Box 1072
Schenectady, NY 12301-1072

10. SPONSOR / MONITOR'S ACRONYM(S)

11. SPONSOR / MONITOR'S REPORT NUMBER(S)

12. DISTRIBUTION / AVAILABILITY STATEMENT

Approved for public release; distribution is unlimited.

13. SUPPLEMENTARY NOTES

*SFA, Incorporated, Crofton, MD 21114

14. ABSTRACT

This report documents the development of a hybrid device for simultaneous 3-axis vibration reduction. This device was found to deliver ~30 to 45 dB downstream vibration reduction of both single and multiple tones. It is robust, reproducible, and sufficiently well-behaved that it can achieve this high performance level using just a base acceleration minimization. A key to its high performance is the ultra-low distortion provided by the highly linear single-crystal piezoelectric actuator. This report summarizes the design procedure, development, and results for what may be the first fully successful small-size 3-axis hybrid actuator.

15. SUBJECT TERMS

Control of acoustics

16. SECURITY CLASSIFICATION OF:			**17. LIMITATION OF ABSTRACT**	**18. NUMBER OF PAGES**	**19a. NAME OF RESPONSIBLE PERSON**
					Peter C. Herdic
a. REPORT	**b. ABSTRACT**	**c. THIS PAGE**	UL	66	**19b. TELEPHONE NUMBER** *(include area code)*
Unclassified	Unclassified	Unclassified			(202) 404-8265

Standard Form 298 (Rev. 8-98)
Prescribed by ANSI Std. Z39.18

CONTENTS

HYBRID ACTUATOR FOR 3-AXIS CONTROL

INTRODUCTION

Scope of this Report

This report summarizes the design procedure, development and results for what may be the first successful 3-axis hybrid (passive-active) actuator.

The previous report in this series, *Hybrid Actuator for Single-Axis Control*[1], described the design, development and successful implementation of a single axis hybrid actuator using piezoelectric materials. It identified the requirements for the hybrid-actuator, and described the parameters, procedures and methodology used to design and fabricate a single-axis evaluation device. Results for the single-axis device were presented and discussed.

The primary objective of the work described here is to extend this earlier work to the more complicated (and important) case of three-axis control. We describe the development, design and fabrication of hybrid actuator devices that demonstrate simultaneous isolation performance along three excitation axes.

This present report is considered an extension of the previous Single-Axis report. The numerical models and design considerations contained in the previous report are not repeated here.

Summary of Previous Report

The single axis hybrid actuator used a conventional passive rubber isolation layer in series with a piezoelectric actuator to isolate a vibrating system from its support structure. Using information provided by sensors, the actuator was driven in such a manner as to reduce vibrational coupling to the lower mounting platform, often called the base or floor.

The sensors (force and velocity) and actuators were essentially in-line and co-located. The force sensor and the actuator were fabricated from piezoelectric materials, while the velocity sensor was a commercial accelerometer.

The force and velocity sensor output voltages were used as inputs to an electronic controller that determined the drive voltage to the actuator layer. Feedback and/or feed-forward control methods were used to implement the control laws selected.

For the single-axis device, the piezoelectric element predominately controls the dynamics of the hybrid system over its frequency range of operation. The passive rubber isolator serves four purposes supporting this operation:

- It assigns the spring constant of the system, forcing a predictable and well-behaved relationship between velocity and displacement
- It provides lateral decoupling, which is not otherwise addressed in this 1-D device.

Manuscript approved May 19, 2006.

- It provides isolation at high frequencies, beyond the frequency range of the active component, which improves the robustness of the control system.
- It provides a safety backup should the active component fail.

From a practical point of view, hybrid isolation of vibrating equipment on a platform would require multiple (e.g. four) single axis hybrid-actuator units. For the single-axis device approach, control of each unit can be addressed independently. This is commonly referred to as local (rather than global) control. It greatly simplifies the control system in applications for which it is suitable.

System goals, performance levels, and static mechanical requirements were discussed in detail in the previous report[1]. The load range was identified as 12 lbf in both axial and lateral directions. Performance was required in the frequency range from 40 to 500 Hz, with the narrow-band noise fundamental near 50 Hz of particular importance.

- The principal conclusions from the previous single-axis hybrid actuator study were:
- Harmonic distortion is significantly reduced (by a factor of 4) by using a “hard” (PZT-4) rather than a “soft” (PZT-5) type ceramic actuator.
- Harmonic distortion is further reduced (by another factor of 4) using the LMS control algorithm.
- The best “system on” performance (24 dB greater than rubber isolator) is achieved when the actuator is located above rubber isolator and acceleration is minimized below rubber isolator.
- The force sensor is not particularly useful for control in single-axis devices.

These requirements and lessons learned were carried forward into the tri-axial work described here.

Components Previously Used

The single axis hybrid actuator was made of several components including sensors, actuators, compliant pads and structural elements. A brief review of the components used in the single-axis device is in order, since many of these are again used in the tri-axial studies.

The laboratory studies and demonstrations reported here and in the previous study use only a single hybrid-actuator unit. Essentially all of the information required at this phase of the development can be obtained by studying the dynamics and controllability of this single unit. Following the single-device tests, the device fabrication can be duplicated as needed for future multiple-device studies and applications.

Passive Rubber Isolator

The hybrid actuator includes a rubber layer. This layer sets the baseline (passive) mechanical impedance of the device, which largely defines the mechanical operating environment.

The dynamic mechanical environment is largely specified by the characteristics of the rubber isolator selected. The reference used for performance comparisons in the single-axis hybrid actuator studies was the Navy Type 11M15 mechanical isolator. It has a dynamic spring constant of 210 lb/in. When loaded with its rated mass of 12 to 15 lb, the isolated system will then have a classical spring-mass resonance at a frequency near 15 Hz. The passive rubber component in the single-axis hybrid device tested was designed to nominally match this spring constant.

While there are a large number of isolator approaches possible, for the single-axis hybrid device study we chose to use the simplest design, consisting of a simple pad of rubber. Because the height allowance and spring constant are both very low, a very soft rubber had to be used. The solid rubber

selected had a measured Shear modulus value of 0.126 MPa. Since the material was very soft, it had a Poison's ratio very close to 0.5, and a Young's modulus value three times that of the Shear Modulus. The variation in the rubber dimensions and properties under load was also studied and the dimensions used for the rubber component were selected with this in mind.

Actuators

The actuator requirements were identified from the system data provided. The maximum displacement required was 0.32 mm, and the maximum force was 1100 dyne. A wide variety of actuator candidates were considered for this application. Considering the modest range of actuation, high force required, and the need for reasonably high linearity, the actuator type selected for this application was a piezoelectric stack.

The maximum voltage that can be applied to the piezoelectric stack is limited by the maximum field strength of the material. This parameter is available from the material manufacturers. A goal of the actuator design was to maintain the overall voltage applied to the actuator to less than a few hundred volts.

Nonlinearities were also considered, particularly as related to observed amplitude-dependent material properties, and hysteresis. Non-linearity is an important parameter since under drive conditions it generates harmonic distortion. Loss contributes to reduced maximum drive levels via self-heating and is loosely related to nonlinearity. It was observed that "soft" PZT materials have substantially greater damping and nonlinearity than hard materials at high fields.

One way to quantify linearity is using total harmonic distortion (THD). This can be measured by driving the transducer with a single-frequency sinusoidal voltage. Displacement (or thickness-change) is then typically measured using an attached accelerometer. With high fields (i.e. 200 V/mm) we typically measure approximately 2 % THD for the "hard" PZT formulations (i.e. PZT-4 and PZT-8), and 9 % THD for the "soft" formulations (i.e. the PZT-5 series).

The actuator finally used for the single-axis study was an NRL-fabricated eight-layer PZT-4 stack. This was found to provide a substantial reduction in material damping and harmonic distortion over the softer PZT-5 stack. This stack was fabricated as a one-of-a-kind laboratory actuator.

Force Sensor

The force sensor has many requirements in common with the actuator, including high static load and shock survivability, good linearity, low drift and small time delay. A particularly difficult requirement to satisfy is the minimum detection limit. Because of the very low forces present, the noise floor of the sensor must be below 0.045 dyne, or -127 dB re: N over the control band (20 to 1000 Hz), and 20 dB lower over the performance band (40 to 500 Hz).

After a review of available force sensors, piezo-rubber type PR-305 (NTK Spark Plug, Int.) was selected for this element. The sensors, as fabricated at NRL, typically had a surface area of 1 sq. in. They consisted of two layers of material, each 49 mils thick and connected in a differential configuration. They have a nominal sensitivity of 0.33 V/N, and a noise floor of 0.64 dyne over a 2 kHz bandwidth.

Because of the rather low capacitance of the sensor, the cable length must be short. Typically a charge-type preamplifier is located within 25 cm of the sensor.

Acceleration Sensor

The noise floor requirement for the accelerometers is quite restrictive. Over the control band the noise floor must be at least 30 dB below (3 % of) the lowest level expected, or 3.6 μg /√Hz; over the performance band it should be at least 20 dB lower. The accelerometers were also required to be small, which was difficult to match to the above very low noise requirements.

While accelerometers meeting these requirements are commercially available as special orders (and have been fabricated and used for other NRL studies), for our previous and present laboratory measurements this was unnecessary. Because the accelerometers were not embedded in the device, but rather were mounted on external components (the top mass and at locations on the supporting base), size was removed as an issue. The accelerometer chosen was then the Wilcoxon Model 759. It had a sensitivity of 100 mV/g with a noise floor of 0.3 μg /√Hz.

TRIAL NON-INSTRUMENTED DEVICE

The study of a 3-axis device was initiated with a trial concept. The purpose of this initial test-unit was to identify the issues involved in moving to a 3-axis device. In particular it was fabricated to explore the mechanics associated with 3-axis rubber isolation and as a visualization tool for exploring the interactions of actuators and sensors.

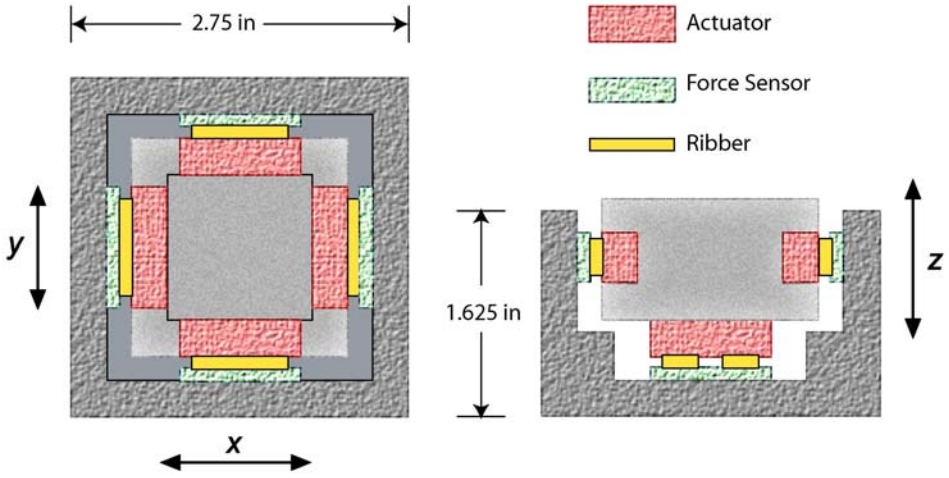

Fig. 1 — Initial test unit design

The device design and placement of parts is shown in
Fig. 1. A unit for mechanical testing was fabricated using Plexiglas for all components except the rubber isolators. These were formed using the rubber material previously documented. A photograph of this test unit is shown in Fig. 2.

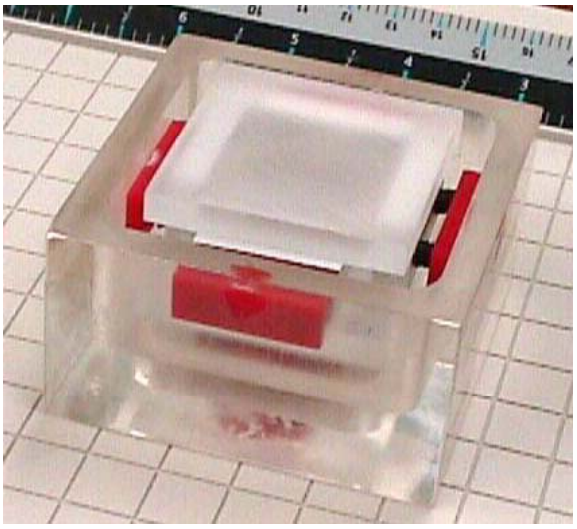

Fig. 2 — Initial test unit for mechanical evaluations

Rubber components

The rubber components were designed using the equations previously presented[1], but with the following additional consideration. For this 3-axis device, the effective spring stiffness in any direction is the sum of the contributions of all components with compliance in that direction.

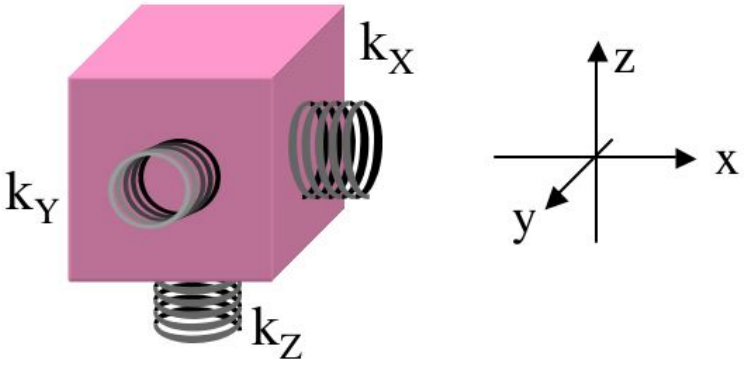

Fig. 3 — Equivalent spring geometry

Consider the equivalent geometry shown in Fig. 3 which contains one spring element on each axis. We define γ as the ratio of the shear to longitudinal stiffness in each spring axis:

$$\gamma = {k(shear)}/{k} \tag{1}$$

where k is understood to be the longitudinal spring constant unless otherwise specified. Then the effective spring constant in the z direction, for example, is

$$k_z(total) = k_z + \gamma_x k_x + \gamma_y k_y \tag{2}$$

where k_x, k_y and k_z are the isolated (longitudinal) spring constants of the springs oriented along the corresponding axis.

Table 1 — Strain Coupling Matrix

Strain direction \ Spring direction	X	Y	Z
x	1	γ	γ
y	γ	1	γ
z	γ	γ	1

For the present case of interest, the spring constants are identical on each axis. This can be represented by the strain-coupling matrix shown in Table 1. Then along any axis i:

$$k_i(total) = k_i(1+2\gamma) \tag{3}$$

The value of γ depends on both material and dimensions. For the type of rubber springs used here, γ has a value of approximately 1/3. Then we can see that 40 % of the stiffness along any axis comes from the contributions of springs oriented along the other axes.

This is only a minor complication to the spring design. It can easily be accommodated using dimensions for the rubber components that appropriately reduce their individual spring constants.

Force Sensor Issue

The above treatment has more important implications for the force sensor, which typically is attached to one side of the rubber isolator. (The accelerometers are unaffected since they are typically positioned externally on the mass and the support.)

First consider an external disturbance applied along the z-axis. Only 60 % of the strain is carried by the z-axis rubber isolator; hence the attached z-axis force sensor will detect only 60 % of this initial disturbance. This sensitivity reduction is unimportant, since it can be included in the calibration.

However each remaining 20 % is carried by the cross-axis (x and y) rubber isolators. While these cross-axis strains are in shear, they generate longitudinal strains in the rubber due to its low modulus. Hence even if the force sensors were designed to be insensitive to shear loads, the x-axis and y-axis sensors would still detect these spurious lateral strains. They would respond by sending a signal to the controller, causing it to drive the x-axis and y-axis actuators in an attempt at compensating for this incorrectly perceived disturbance.

For these lateral sensors, the influence of these cross-axis sensitivities can be reduced by various techniques. Perhaps the simplest approach (used here) is to use pairs of sensors on either side of both the x- and y-axis, as illustrated in Fig. 1. The pair would be wired as a single differential sensor. This provides twice the sensitivity to true lateral motions, while tending to suppress spurious signals (which are generated equally in both), as detailed later.

Unfortunately the issue is not as easily handled for the z-axis. Since the loaded surface is laterally unconstrained, a differential pair of sensors would not be useful. Some additional design feature is required to remove the cross-axis sensitivity on the z-axis sensor.

Results

The conclusions from this exercise are:

- The rubber isolator design equations were confirmed by laboratory measurements to reliably predict the dynamics of the structure.
- The presence of cross-axis compliance can be easily accommodated in the rubber component design to achieve the required total effective spring constant.
- The x and y axis force sensors should be installed as matched differential pairs to help discriminate against cross-axis coupling.
- Attention must be paid to the adhesives used in the x and y axis force sensors, since these support the full static load in shear.
- For this first design, cross-axis coupling for the z-axis force sensor is a serious unresolved issue.

Although this first design would not yield a practical device, the lessons learned proved useful in the design of the first fully-outfitted test article.

FIRST FULLY-OUTFITTED TEST ARTICLE

A number of possible solutions to the z-axis cross-coupling issue were explored. The most promising appeared to rely on floating the x-y stage in some manner that filters lateral motions from the z-axis sensors.

Approach

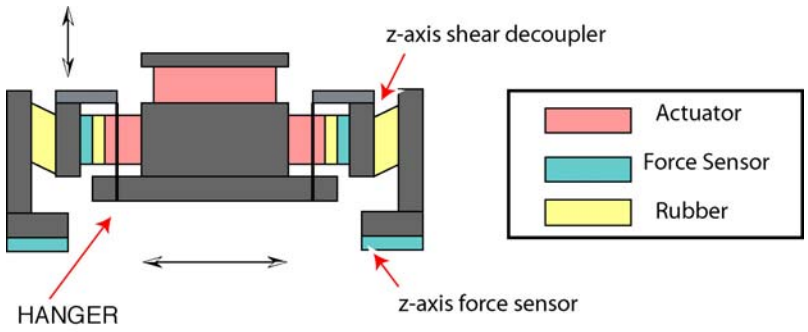

Fig. 4 — Design of first operational 3-axis device

The design selected is shown in Fig. 4. As usual, the connections to a top-mass and bottom-support are not shown. If we focus first on the rubber components, the design separates into three sections: an outer-frame, an inner-frame, and a central-piston. The rubber isolator between the inner-frame and central-piston is a rubber pad strained in the thickness or longitudinal direction, similar to that used previously. The rubber isolator between the outer-frame and inner-frame is a rubber pad strained in the shear direction (shown exaggerated in the illustration). This will be referred to as the "z-axis shear isolator."

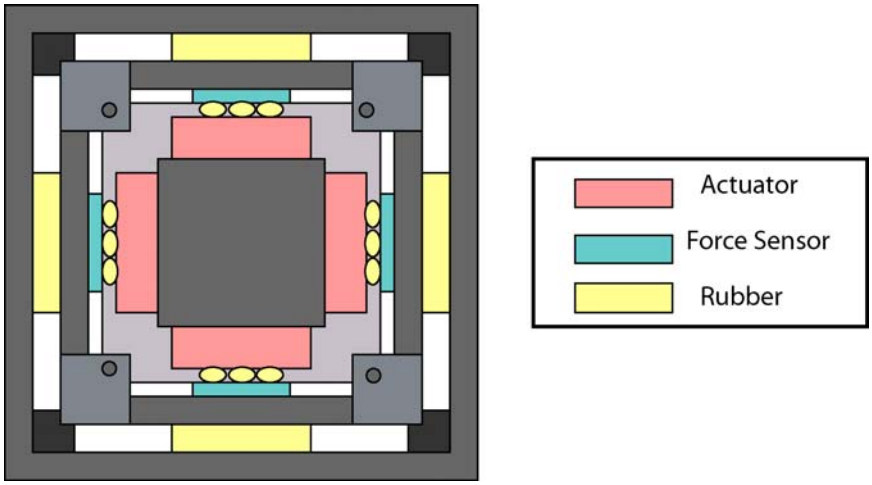

Fig. 5 — Top view of device

A top view of the device is shown in Fig. 5. This view more clearly shows the frame-within-a-frame construction and the central driver block, often referred to here as the central-piston.

The x and y axis components connecting the inner-frame and central-piston are similar to those shown previously, where the actuators are bonded to a central-piston, the force sensors are bonded to the inner support frame, and the actuators and sensors are connected using longitudinally-strained rubber isolators.

The z-axis is somewhat different. The z-actuator is positioned on the upper mounting surface of the central-piston, and the z-axis force sensor is positioned on the bottom of the outer-frame. This is in keeping with the recommendations from the previous single-axis study.

The key new feature in this design is the presence of an inner frame, and the use of a hanger connecting the inner-frame and central piston. This hanger is free to rotate, but supports the full vertical load on the central-piston. This feature has two results:

- Of greatest importance, it suppresses certain terms in the cross-coupling matrix.
- Of lesser importance, it relieves the static shear load on the force sensors.

The mechanical operation of this system can be described by first considering the application of a vertical force on (or applied by) the z-axis actuator. The inner-frame and central-piston are locked together vertically through the hangers. Hence all vertical force applied to the top is transferred to the inner frame. The z-axis components are therefore entirely separated (in the ideal case) from the x- and y-axis components.

Now consider the application of a lateral force. To simplify this exercise, it is more useful to consider the application of this lateral force to the support base of the unit. Since the force sensors are considered stiff, the force transfers to the outer-frame. The z-axis shear isolator is also relatively stiff in this lateral direction, which is its thickness or longitudinal direction. Hence most of the force transfers to the inner-frame. There it is sensed and acted-on by the usual x- and y-axis components.

The net result is that the z-axis components are (to some degree) isolated from the x- and y-axis stage.

Cross-Axis Compliance

While the above design substantially reduces the cross-axis coupling, particularly in the troublesome z-axis, some additional improvements were desirable.

X and Y axis

The x and y axis coupling is still significant. A strain along either axis generates a corresponding strain along the other axis. Recall that the simple (thick) rubber isolator has a value for the coupling parameter of $\gamma \sim 0.33$. The relative magnitude of the cross-axis strain is approximately one third (or 10 dB down from) the original strain.

Potentially the most detrimental result of this would be on the accuracy of the force sensors. However as previously mentioned the magnitude of this error signal can be suppressed by using a pair of sensors, wired differentially. The degree of suppression will be limited by the degree to which the sensors are matched. Assuming that the two sensors are matched to within 10 % (a good figure for piezoelectric transducers), this would provide a maximum of 20 dB of suppression.

A better solution, however, is always to reduce potentially troublesome interferences at their source. One approach considered is replacing the simple rubber isolator pad with an isolator having a lower coupling parameter γ.

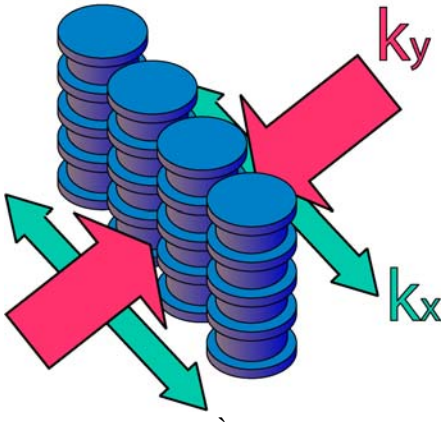

Fig. 6 — Ribbed rubber cylinders isolators

After considering various options, the approach selected is to use a configuration we refer to as "ribbed rubber cylinders." The geometry is shown in Fig. 6. These were fabricated from the same soft rubber as used previously. As expected, the stiffness in the longitudinal or thickness direction (y in the figure) is little changed over that of a rectangular pad of comparable dimensions. However the shear stiffness of these isolators is very low. The value we measured for the coupling constant of this isolator is $\gamma = 0.05$.

This is a substantial improvement over the simple rubber pad. These are used as the isolator element only on the x and y axes. They also have relatively low stiffness in the z-direction, ensuring the vertical load is supported primarily by the hangers.

Z-axis isolator

For the z-axis isolator, we chose to use a vertically-oriented rubber pad in shear to provide the desired stiffness. This selection provides low stiffness in the vertical direction while encouraging a high stiffness in the lateral direction.

In the design model, the longitudinal and shear spring constants are calculated for each rubber pad. These are then combined to obtain the net spring constant for each direction axis. The design equations used for the longitudinal spring constant were presented in the previous report in this series. The shear spring constant k_s can be described using the familiar equation

$$k_s = G\frac{A}{t} \tag{4}$$

where G is the Shear modulus, A is the loaded surface area, and t is the thickness of the layer undergoing shear. In some applications the shear modulus value must be adjusted for the shape factor (as previously done with Young's modulus). The effective shear modulus in such cases is then given by

$$G_{eff} = \frac{G}{1+\frac{1}{3}\left(\frac{r_g}{L_s}\right)^2} \tag{5}$$

where r_g is the radius of gyration of the shear cross section about the neutral axis (r_g = 0.2887 t), and L_s is the length of the side corresponding to the neutral axis.

The total shear spring constant will be the sum of the spring constants for all four (identical) rubber pads. The x-y isolators do not contribute in this case, since they do not carry the vertical load.

An issue with this z-axis isolator is that, for the present application, the stiffness in the lateral direction is not as high as we would like. Lateral compliance in the z-axis isolator would reduce the force sensor sensitivity, but more important, could contribute cross-axis compliance.

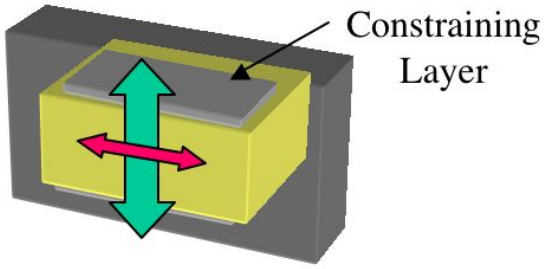

Fig. 7 — Lateral stiffening of the z-axis shear isolator

The approach selected for use here is to stiffen the z-axis isolator by adding a constraining layer. This is illustrated in Fig. 7. The constraining layer used in our tests is 50 micron (2 mil) thick nickel. The value γ we measured for the coupling constant of this isolator is 0.11. This is approximately a factor of three improvement, and is adequate for our studies.

Fabrication

Actuators and sensors

The actuator used in this device is a PZT-8 stack, custom-fabricated by International Transducer Corporation (ITC) to NRL specifications. PZT-8 was selected because it has even lower damping (and presumably higher linearity) than PZT-4. Like PZT-4, it is a hard ceramic. While PZT-8 has 30 % less displacement per volt, it can be driven at higher voltage levels to compensate, if necessary.

The stack is formed from 10 active wafers, where each wafer is 0.635 mm (25 mils) thick. Two additional inactive wafers are used a cover plates. The total thickness is 7.87 mm (0.31 inch).

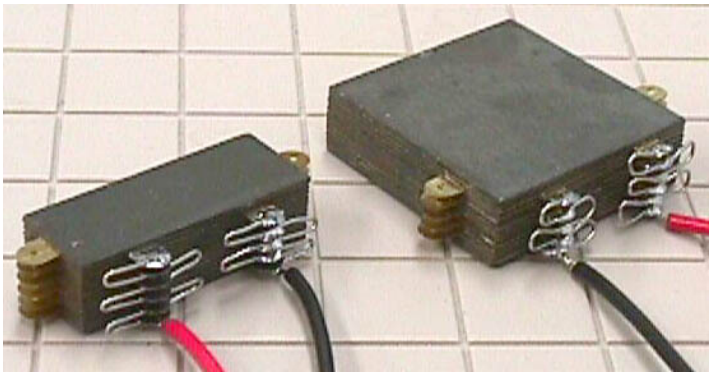

Fig. 8 — Actuator stacks from ITC

Table 2 — Properties of stacks delivered (manufacturer's data)

Size	Serial	Capacitance (nF)	Dissipation	Resonance (kHz)	
				F_m	F_n
1” x 1”	1	103.0	0.40 %	72.13	80.90
	2	101.6	0.40 %	71.85	81.05
0.375” x 1”	1	39.4	0.40 %	64.55	67.55
	2	39.1	0.40 %	65.00	67.78
	3	40.2	0.40 %	65.33	67.63
	4	40.3	0.40 %	65.48	67.83
	5	39.6	0.40 %	64.65	67.53
	6	40.2	0.40 %	64.78	67.33

Two different-size actuators were used in this device, as shown in Fig. 8. For the z-axis, the actuator was 25.4 mm (1.00 inch) square. For the x and y axis, the actuators were 9.5 by 25.4 mm (0.375 by 1.00 inch). Some properties of these stacks are listed in Table 2, where F_m and F_n are the first anti-resonance and resonance frequencies of the free stack. These were used in pairs on opposite sides of the central-piston.

The actuators stacks were designed to deliver 2.3 nm per volt displacement. The initial batch of actuators delivered by ITC were measured and found to have no net displacement output. Laboratory tests at NRL (destructive and non-destructive) found that each wafer was correctly delivering the correct displacement, in the range 222 to 252 pm/V. However the displacement direction of the wafers were alternating. This indicates that the wafers were incorrectly assembled, with all wafer polarities aligned rather than alternating. Hence there was no net displacement between the top and bottom surface. The

manufacturer replaced all stacks with a new batch. Laboratory tests then confirmed the expected nominal 0.46 micron displacement when driven at 200 V.

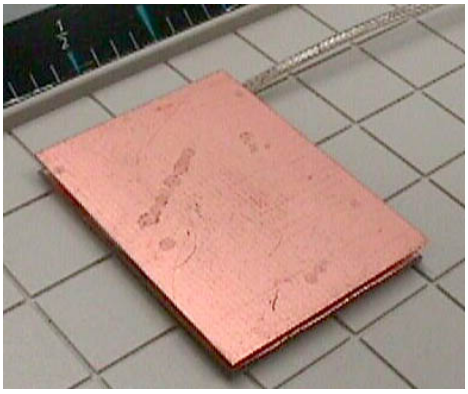

Fig. 9 — Typical force sensor

The force sensors were again fabricated at NRL using NTK PR-305 Piezo-rubber. Each was a two-layer stack of 1.27 mm (50 mil) material, wired using the usual alternate-polarity configuration to provide electrical shielding and reduce noise. As described in the previous report[1], expanded wire mesh was used to connect the sensor layers and ensure their electrical contact to the copper-platted GRP boards located top and bottom. These boards also provided additional shielding, surface protection, and convenient points for electrical contact.

Two different size force sensors were also needed. For the x and y axes, the sensors were 25 by 10 mm (1 x 0.40 inch), and had a sensitivity of 146 mV/N. For the z-axis the size was 89 by 6.4 mm (3.5 x 0.25 inch), and had 68 mV/N. In both cases the noise floor was near 10 μN over a 2 kHz bandwidth.

As previously mentioned, the accelerometers were located external to the device, on the mass and on the support platform. They were typically Wilcoxon Model 759.

Assembled device

The device was fabricated using aluminum for the frames. An exploded view of the device is shown in Fig. 10.

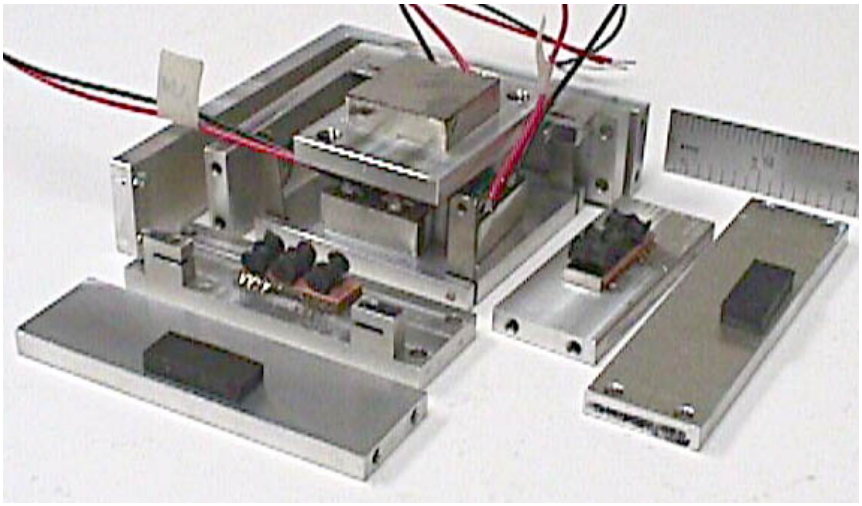

Fig. 10 — Exploded view of first operational 3-axis device

The outer-frame is shown with two sides removed. The z-axis shear rubber isolator is shown attached to the outer-frame pieces. (The constraining layers are not installed.) The inner-frame is also shown with two sides removed, and with the force sensors and ribbed-rubber cylinders attached. The center-piston has all five actuators installed and wired.

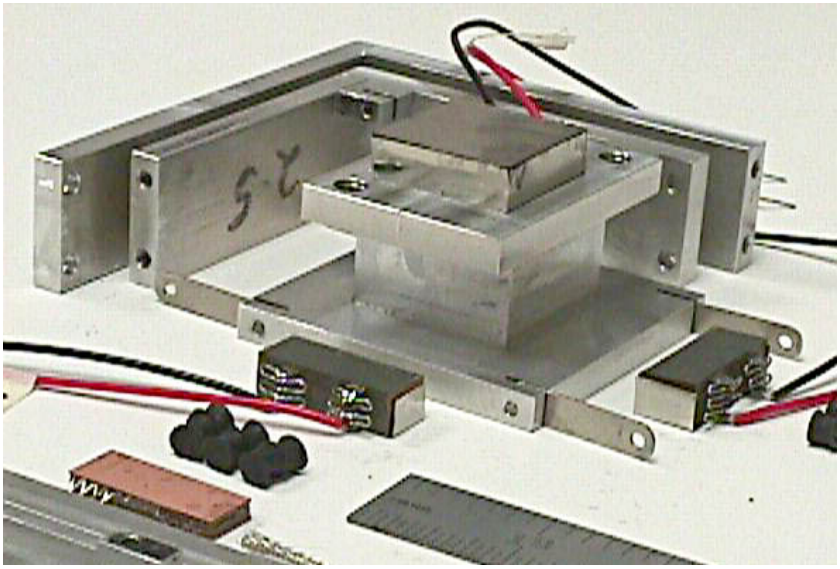

Fig. 11 — Exploded view showing center piston prior to actuator installation

Fig. 11 shows a closer view of the device before the lateral actuators were installed on the central piston. The hangers are shown attached to the center-piston, but lying horizontal. The ribbed-rubber cylinders and force sensors are also more clearly seen.

Hangers

Initially the hangers were fabricated from wire. However these proved unsatisfactory since their lengths could not be accurately matched. Instead, as shown in the photograph, hangers were fabricated from 20 mil thick stainless steel shim stock. The holes in these metal hangers were oversize to allow ample rotational freedom, but accurately matched to hang at nominally the same height. These were attached by metal pins, which were press-fit into holes in the inner-frame and center-piston. The hangers were observed to be free to rotate about the pins, and had low bending stiffness. Hence they exerted little constraint in any but the vertical direction.

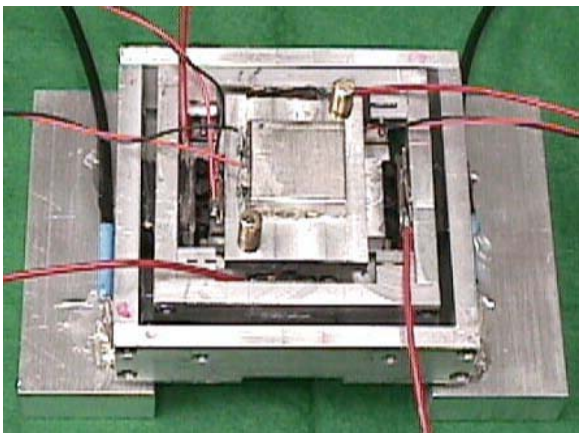

Fig. 12 — Fully assembled device (resting on two supports)

Laboratory Test Fixture

As a single unit, the device is not easily evaluated. Special evaluation apparatus must be constructed to reduce unwanted moments.

In practical applications multiple supports (i.e. four corner supports) are used and the motions are typically axial or lateral. Any rotational or torsional compliance is unimportant since these are constrained by the presence of multiple supports. For evaluating a single device under load, however, the torsional moment is only lightly constrained. This is depicted in the cartoon of Fig. 13.

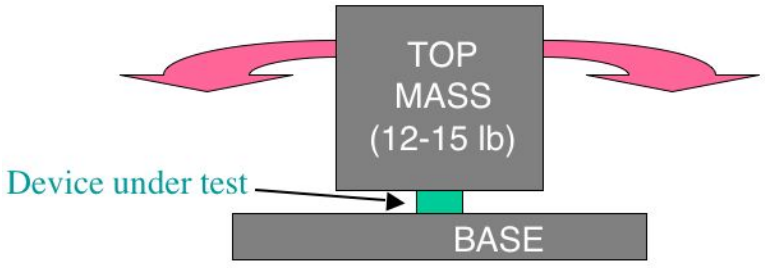

Fig. 13 — Cartoon illustrating the evaluation issue

A variety of different laboratory arrangements were developed and tested, including some with point constraints on the vertical and/or horizontal axis. The results led to the apparatus arrangement

shown in Fig. 14. In this figure, one side of the top mass has been removed to show the device positioned inside on two supports.

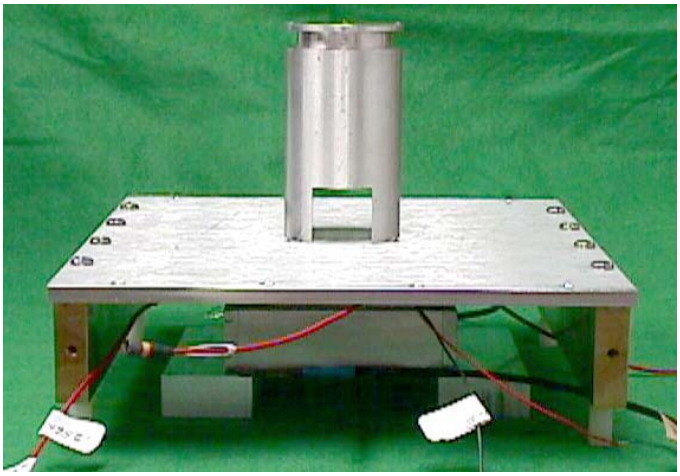

Fig. 14 — Device in test fixture

The important feature is that the center-of-action of all masses and actuators should be centered to minimize extraneous mode excitation. Hence:

- The top mass is dropped as an encircling frame, with the center-of-mass located at the center of action of the device.
- Threaded nylon feet are also included to provide the option of forming light contact with the base to provide a slight torsional constraint. (This was occasionally used only with this present version of the device.)

The use of additional motion constraints on the fixture was found to be counter-productive.

For actual evaluations, the above assembly was placed on a platform that was isolated from the building floor using air mounts, as described in the previous report[1]. A representation of this test setup is shown in Fig. 15.

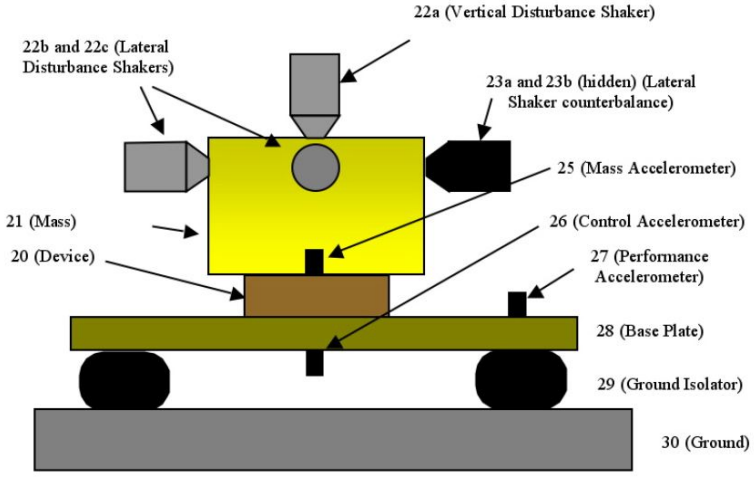

Fig. 15 — Cartoon showing laboratory evaluation components

The device was loaded with a 5.6 Kg mass. Three disturbance shakers were located on the mass, one vertical and two lateral. Small masses were added to counterbalance the mass of these lateral shakers. The total mass supported by the device under test was then 7.718 Kg (17 lb). The entire assembly was supported on a 12.6 Kg base plate, which was isolated from the ground using soft air mounts having a spring constant of 103500 N/m.

Note that to simplify the illustration, parts have been exaggerated and the mass is shown located above the device under test. As mentioned, in the actual test arrangement the mass is configured to have its center-of-mass located on the centerlines of the device under test. For single-device testing, this reduces test anomalies related to the low rotational stiffness associated with the test arrangement. This consideration is not an issue for anticipated applications, where typically three or four such devices (acting independently) support a platform, providing inherent rotational support stability.

Tri-axial accelerometers were positioned at three locations. The mass-accelerometer was mounted near the vertical centerline of the mass and used to monitor the tri-axial disturbance amplitude. The base or control-accelerometer was mounted on the base plate directly under the center of the device under test. Its output was used as the sensor input to the controller, and during controller operation the controller attempted to minimize this sensor output. The performance-accelerometer was mounted at a down-stream location on the base plate to monitor the isolation performance obtained.

The controller used was quite simple. It consisted of three separate local controllers (one for each axis, with no interconnectivity or shared information). Each local controller was simply a SISO (Single-Input Single-Output) 8-weight FIR (Finite Impulse Response) digital filter. As discussed in the previous report in this series, one factor influencing the complexity or simplicity of the controller is the linearity of the mechanical system, and particularly that of the actuator. Nonlinearities in the actuator generate harmonic distortion, which typically require more complex controllers to reduce out-of-band enhancement. In the above design, the relatively linear PZT-8 actuator material was selected (rather than, for example, a more efficient but more non-linear material such as PZT-5). This selected material has low hysteresis and low harmonic distortion. Hence even with the simple controller used in the demonstration, there was found to be less than 0.5 % out-of-band enhancement.

Laboratory Results

Laboratory results for this first test article were initially promising but the overall performance obtained was inadequate. Typically 15 - 25 dB reduction would be obtained on two axes, but little if any reduction would be found on the other.

The limiting performance issue in this first test was that the cross coupling was significantly higher than anticipated. This was traced to the hangers, and particularly to the square geometry and the choice to use four hangers. The mechanism is related to the very small displacements involved, which are typically a small fraction of a micron. Since the hanger lengths are not matched to this precision, and the platform is stiff, it was recognized that the central-piston will only be supported by three hangers at any given time. Two of these hangers will be diagonal. Any disturbance leads to an instability in the form of an unrestrained (or very lightly restrained) rocking moment about the two diagonal support hangers. This invariably couples energy into the lateral directions.

A simple modification was incorporated in an attempt at removing this instability. The steel pins holding the hangers were replaced with nylon pins. The nylon was sufficiently deformable that all four hangers shared the load more-or-less equally. With this modification the cross-axis coupling term was significantly improved.

The subsequent laboratory results were improved and occasionally excellent. Some runs demonstrated 10 to 15 dB reduction simultaneously on all three axes, and one run achieved 20 dB simultaneous performance on all axes. However this performance was often not reproducible. Small changes in the alignment of parts, or even the settling of parts with the passage of time, would degrade this performance.

Discussion

The purpose of this first laboratory 3-axis device was to guide us in determining the important design features and performance levels attainable using a fully-outfitted 3-axis device. This version of the device was not designed to be practical, being complicated, expensive and fragile. Instead it was designed for laboratory explorations. Its most important features are:

- It was fully instrumented with sensors for power flow studies.
- It contained linear, high performance actuators for precise displacement generation.
- It was designed for low cross-axis mechanical coupling.

As such, the device performed admirably. It was useful in identifying design changes and simplifications that would enable a more practical device construction.

- The key findings and results are:
- The mass-centered test setup is essential for evaluating single devices.
- The linearity and performance of the actuator is very good.
- As much as 20 dB of system performance was obtained simultaneously on all axes (but often this high level was not repeatable).
- Rigid bonding of all components is essential to eliminate mechanical leakage.

Perhaps the most important lesson learned from this device is:

- The cost of including lateral force sensors is very high.

REDUCED COMPLEXITY 3-AXIS DEVICE

Approach

Based on the experience and results for the previous device, a more practical device design was developed.

The single most important change was the removal of the force sensors on the x and y axes. The results of our previous studies indicate that control approaches using only the accelerometers yielded better performance that those using the force sensors. Hence the force sensors are now an unnecessary complication.

By removing the force sensors, the device construction becomes considerably simpler. Without these sensors, cross-axis coupling is largely eliminated as a serious issue. Interference from residual actuator EMI was only a factor of relevance to the force sensor, so it too becomes unimportant. The device design can then become much less complicated. This results in a more rugged and forgiving article, which can be fabricated at significantly lower cost.

Concept

An illustration of initial concept is shown in Fig. 16. While the rubber isolators can be designed as either longitudinal or shear, for the present device we chose shear. This is preferable in this application since, for comparable spring constants, shear isolators are generally thinner than longitudinal isolators. Hence the four rubber pads shown connected to the base actually serve predominately as the lateral isolators, and the four connecting the frame to the piston predominately contribute to axial isolation.

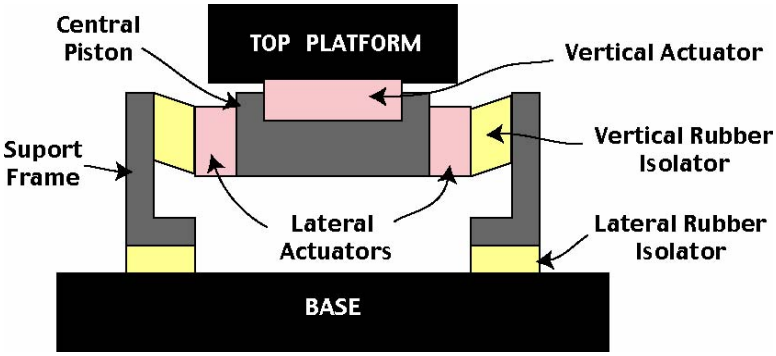

Fig. 16 — Conceptual design of a reduced-complexity device

An important feature is that all eight rubber pads have nearly identical spring constants in both shear and longitudinal directions. Hence the compliance of the device is orientation independent.

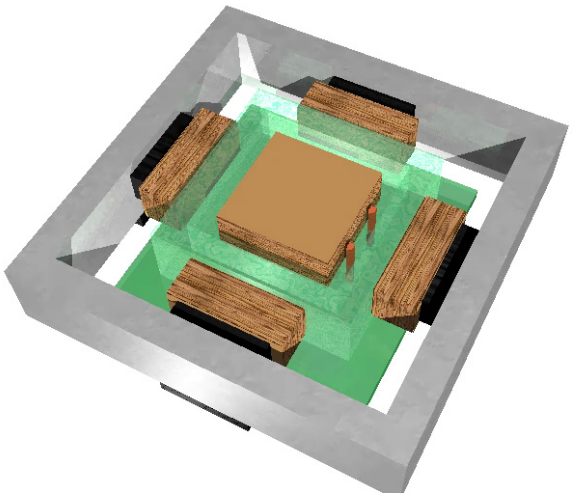

Fig. 17 — Illustration of the initial reduced-complexity device

A three dimensional view of the above device concept is illustrated in Fig. 17. In this figure the actuators are shown as brown rectangles surrounding a central (green) piston. Rubber components are shown in black. As usual, the mounting surfaces are not shown. Such a device is seen to be considerably less complicated than those studied previously.

Concept Refinement

The device illustrated requires one major refinement. For the configuration shown, the center-of-action of the axial and lateral rubber isolators are not collocated. This can be resolved by splitting the outer frame into two sections. Then the rubber isolators that are shown on the base are repositioned to the interface between the upper and lower frame.

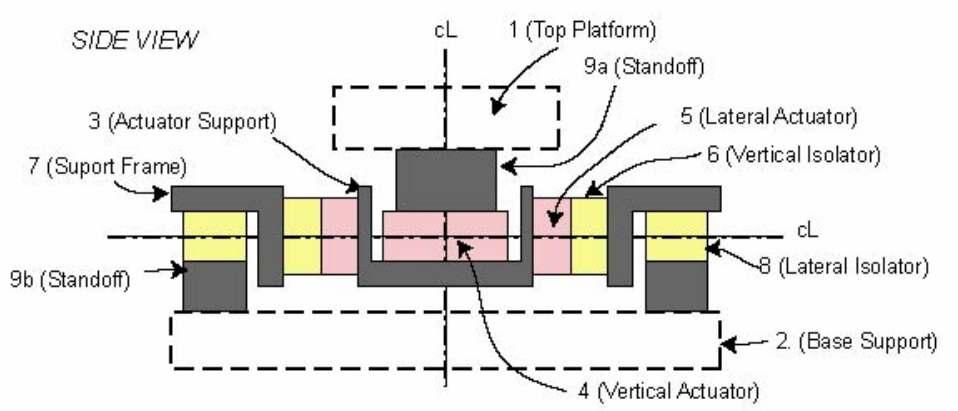

Fig. 18 — Illustrative device configuration (side view)

Fig. 18 and Fig. 19 illustrate a simplified form of the general device configuration. The device is located between a top platform and a supporting base. Standoffs may be included if needed to facilitate positioning.

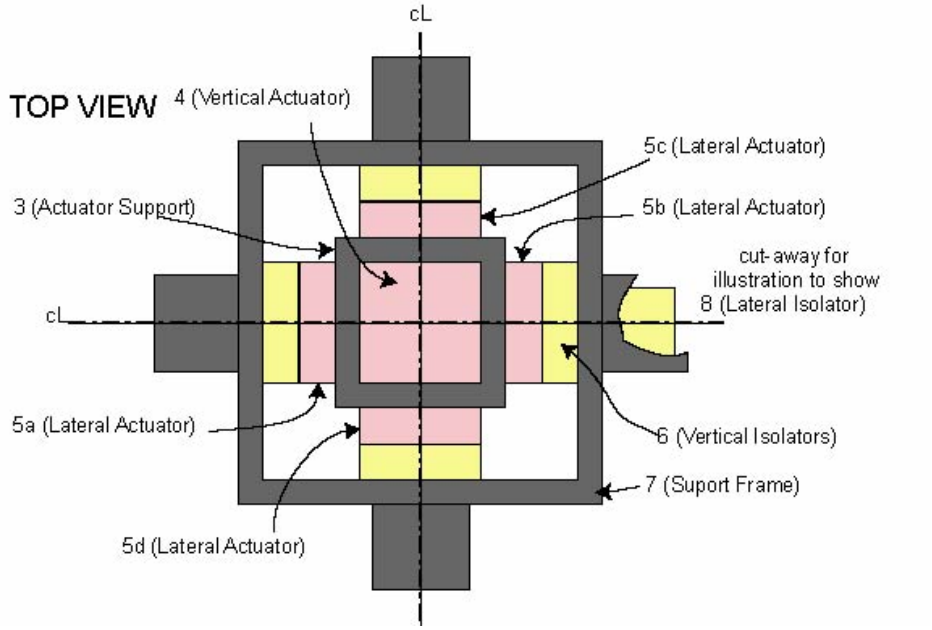

Fig. 19 — Illustration of device configuration (top view)

The device contains an actuator assembly consisting of a vertical actuator and four lateral actuators. All five actuators are mechanically attached to a stiff actuator support block. Three electrical cables (not show) are attached to these actuators, where each cable contains a drive-signal wire and a return. One cable drives the vertical actuator. A second cable drives the lateral actuator pair as a parallel electrical configuration. The electrical attachments to the actuators in this pair are of opposite polarity, such that the actuator motions act in opposition. Hence a positive drive voltage applied by the electrical cable will

cause one actuator to expand and the other to contract. This is often referred to as a push-pull type actuation. The third cable drives lateral actuators, which are similarly wired in opposition as a push-pull pair.

The device also contains a passive isolator assembly consisting of four vertical passive isolators and four lateral passive isolators. These are all mechanically attached to a common stiff support frame. These passive isolators are typically rubber isolation mounts operated primarily in the shear configuration.

Operational features

The passive isolation assembly is mechanically distinct and separate from the actuator assembly and sensor (accelerometer) array. This allows the various passive rubber components to be treated using only lumped parameters. Only the net combined compliance of the passive components is of significance, not their order of placement. Hence, for example, the effective compliance in the vertical direction is a simple combination of the shear compliance of the four vertical isolators plus the compressional compliance of the four lateral isolators. Only this net compliance contributes to the vertical mechanical input impedance experienced by all actuators. The selection of passive isolator characteristics thus becomes a simple location-independent design process.

The passive isolators are all balanced and symmetrically located on the vertical centerline and in the lateral plane defined by the two lateral centerlines, With this location restriction, the net compliance associated with the passive isolator assembly is centered at the intersection of the three orthogonal dynamic-mechanical axes. Forces or motions transferred by these passive components then tend to retain their original directionality. Hence, for example, a force applied to the passive isolator in the vertical direction will tend to remain focused in that direction, and not couple to other axes or moments to form extraneous translational or rotational components of force or motion. Cross-axis compliance of these elements then becomes unimportant.

The lateral actuators are similarly located along the same common orthogonal axes indicated by the centerlines. Hence the forces or motions they apply will tend to remain focused in the applied direction.

Similarly the vertical actuator is located on the vertical centerline, and near or on the plane defined by the lateral centerlines. This ensures that the forces or motions it applies will remain focused in the vertical direction, without significant coupling to the rotational or cross-axis directions. If the device is used in the vertical orientation, a vertical offset of this actuator location along the vertical centerline will not degrade the device performance. However if the device is on a platform such that it may experience significant off-vertical orientations, then the vertical actuator should be located on the true dynamic centerline.

The use of push-pull operation for the paired lateral actuators is also important. The advantage of this can be illustrated as follows using one particular operating mode as an example. Consider the case of a lateral vibrational motion occurring in the top platform, whose displacement magnitude is not significantly influenced by the stiffness of the device. One wishes to operate the actuators to prevent transfer of this vibrational motion or energy to the base support. If a symmetric pair of actuators is available they can be driven to follow this motion of the top platform without applying significant force to the remainder of the device or the base platform. In this case, the energy transfer to the base will be low, and the isolation high. However if a symmetric pair is not used, the actuation of one actuator must apply a force to the actuator support. This energy transfer will limit the amount of isolation available as well as generating an undesirable moment or torque, which will couple to motions along the other axes of the device.

The result of the above is that forces applied in one direction will tend not to generate extraneous forces in any of the other (perpendicular or rotational) directions. Hence the mechanical cross-axis coupling matrix of the actuators and compliant elements is essentially diagonal, with only very small coupling values in the off-diagonal elements.

Device Fabrication

The central piston was machined from aluminum block, and the actuators attached. The actuators used were the same ITC piezoelectric transducer stacks described previously. Because the rubber isolators are used in shear, it is the vertical rubber isolators that are glued to the lateral actuators, as shown in the illustration and photograph of Fig. 20. Since this device will be used only in the vertical orientation, it was permissible (and convenient) to have the vertical (z-axis) actuator positioned somewhat above the lateral center-plane of the device. Otherwise (in the current evaluation apparatus) an additional standoff would be needed on the actuator surface to raise it above its surrounding elements.

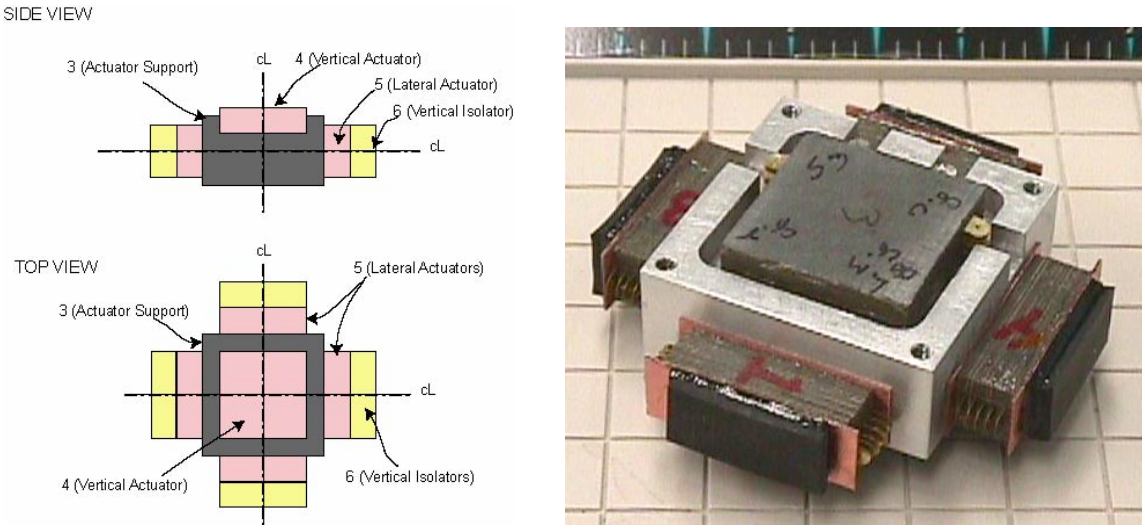

Fig. 20 — Illustration and photograph of the central actuator assembly

The outer frame sections were also aluminum, machined to fit the central actuator assembly as shown in Fig. 21. To connect with the portion of the device shown in the previous figure, the vertical isolators are shown in this figure as well. The vertical isolators were attached to an aluminum frame. The lateral isolators are also bonded to this frame, as well as to a lower supporting frame that serves as a standoff. In this particular implementation, the vertical passive isolators were located in the corner locations, as illustrated.

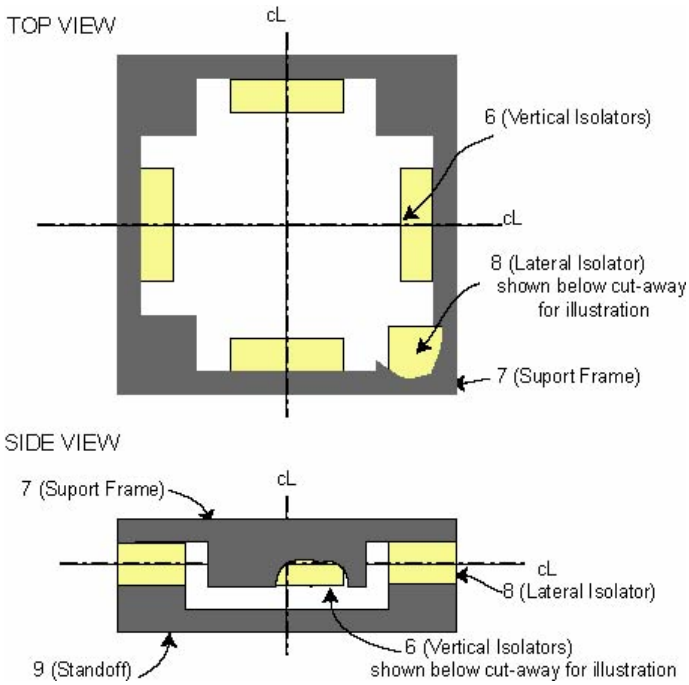

Fig. 21 — Passive isolation assembly

The passive isolators are all rubber pads strained in shear. The spring constant of the total passive isolation assembly should be nominally 30,000 N/m (170 lbf/in) in all three directions, to provide a fundamental resonance frequency of nominally 10 Hz when used with the current 7.718 kg (17 lb) mass. The design involves selecting material dimensions to produce the desired spring constants. The design equations for the individual rubber pads were presented earlier in this report.

The total spring constant is then

$$k_{T,y} = \frac{4}{\frac{1}{k_{S,y}} + \frac{1}{k_{L,z}}} \qquad k_{T,y} = \frac{4}{\frac{1}{k_{S,z}} + \frac{1}{k_{L,y}}} \tag{6}$$

where the first index of the spring constant is S for shear, L for longitudinal, or T for total. The second index identifies the axis: y for the horizontal (x or y axis) or z for vertical (z-axis).

The results for the individual pads and the total system are shown in Table 3. The longitudinal spring constants are seen to be much larger than the shear; hence they represent stiff elements that do not contribute appreciable compliance.

Table 3 — Rubber isolators used in the Reduced-Complexity device.

Isolator	Area	Thickness	Spring Constant		
axis	(mm)	(mm)	Shear (N/m)	Long. (N/m)	Total System
X, Y (Lateral)	15 x 15	3.0	8.8x103	122 x103	30.4x103
Z (Vertical)	10 x 20	3.0	8.1 x103	96 x103	32.2 x103

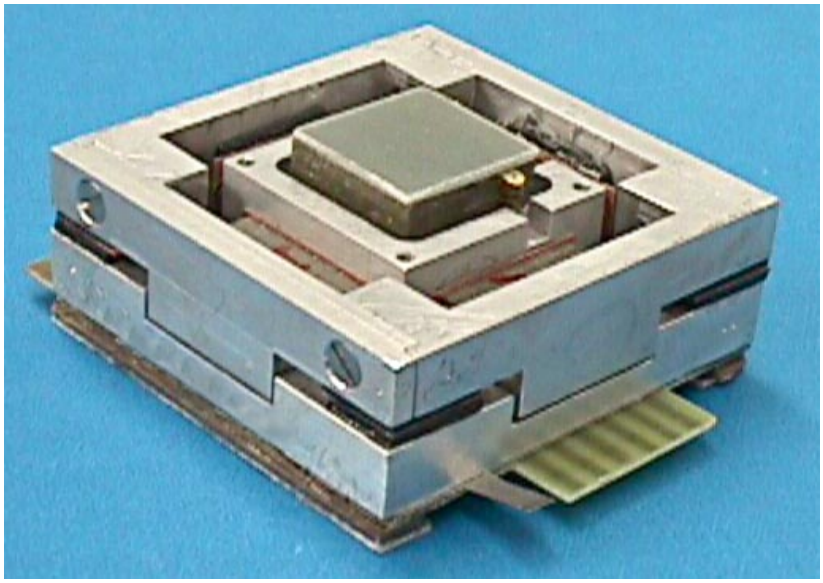

Fig. 22 — Photograph of the device tested

The complete device is shown in Fig. 22. A photograph of the bottom of the fabricated device is shown in Fig. 23. The device shown contains two additional components not previously mentioned. For convenience electrical connections to the drivers use a printed circuit board attached to the base. A force sensor is also distributed along the two edges of the base (and wired in parallel) to monitor the force generated in the vertical direction. Neither of these components interferes with the device operation

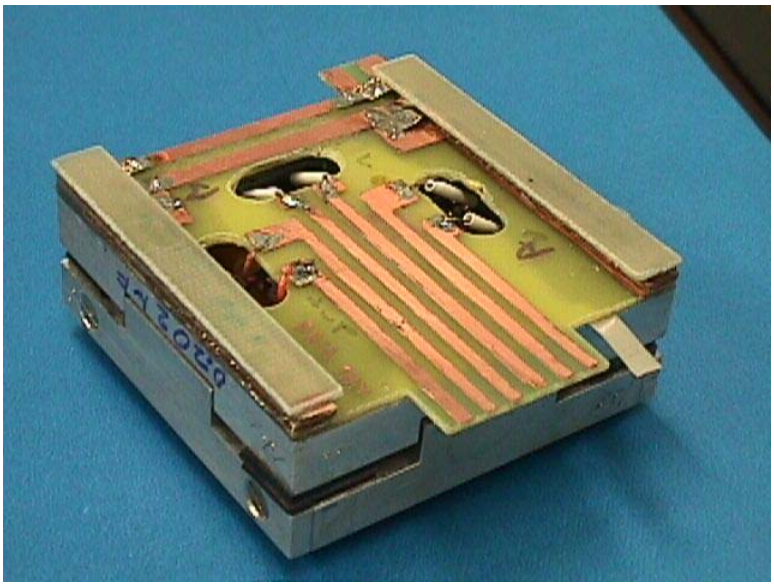

Fig. 23 — Bottom view of the fabricated device

Performance

The device was evaluated in the same apparatus used earlier. Standoffs were used to adjust the height so as to locate the center of the mass at the center of action of the device.

Measurements obtained demonstrate the high isolation that can be achieved with this device. For example measurements at 50Hz with the control system off (actuators not driven) found that the passive isolator alone had a transmissibility of 28 %, or -11 dB. This means that the measured motion of the base plate is only 28 % as large as that of the mass, or the passive isolator prevented 72 % of the mass motion from being transferred to the base plate.

When the control system is turned on, the actuators contained in the device are driven by independent SISO (single-input, single-output) controllers to minimize the acceleration detected by the base or control accelerometer. Under these conditions the motion detected by the base or control accelerometer is at least 50 dB less than that found at the mass.

When so operated the acceleration at the (downstream) performance accelerometer location is that shown in Table 4. As indicated, in the two lateral directions it is nominally 41 dB lower than that of the mass, or slightly less than 1 % displacement transmissibility. In the vertical direction the performance is nearly as good, 34.5 dB lower than that of the mass or slightly less than 2 % displacement transmissibility. This was demonstrated with all three disturbance-shakers (located on the three orthogonal axes) simultaneously vibrating the mass.

Table 4 — Measured performance (all axes simultaneous) at downstream location.

Axis	System Performance (including passive isolator)	Performance Improvement (System On / System Off)
z-axis (vertical)	-34.5 dB	-23.5 dB
y-axis (lateral)	-41.1 dB	-30.1 dB
x-axis (lateral)	-42.0 dB	-31.0 dB

Hence the isolation provided by this first device fabrication is demonstrated to be nominally 35 to 40 dB, corresponding to a transmissibility of only 1 to 2 %. Compared to the 11 dB isolation performance of just the passive isolator assembly, the actuator assembly and its associated control components contribute 24 to 30 dB greater performance.

Discussion

The performance of this reduced-complexity device is very good. In particular it offers:
- 11 dB passive isolation
- An additional 23 to 30 dB provided by control
- Full Three-Axes isolation and actuation
- Package size less than 1 inch thick and 3.5 inches square
- Usable at all orientation angles

The design has a number of innovative features, some of which are the subject of a patent disclosure[2]. The key design features of this device are:
- No lateral (x and y axis) force sensors.
- Separate actuator and passive-isolator assemblies.
- Co-located center-of-action for all passive-isolator components and actuators.
- Lateral actuators wired as push-pull pair.

- Relatively uncomplicated and reproducible fabrication

This device fulfills all of our original design goals, with one exception. It is physically larger than desired. Our final effort in this series was then directed at reducing size, and presumably additionally reducing cost and complexity.

COMPACT DEVICE

While the performance of the reduced-complexity device is excellent, its size is somewhat larger than desired. This is to a significant extent limited by the size of the actuator stacks used.

As identified at the onset, the goal of small size could only be met if we then anticipated the commercialization of a new actuator material during the performance period of this study. The anticipated actuator material was single-crystal PZT materials, then being developed under substantial ONR and DARPA programs.

Fortunately, as anticipated, this new actuator technology became commercially available in 2003. Hence it was available in time to be used in the final device design of this series.

Actuator Material

Single-crystal transducer materials are quite recent, yet because of the rather large programs supporting their use there is an appreciable amount of information available.

The advantages of using single-crystal material are:

- Very high displacement per volt for a ceramic material (10 times higher than PZT-8)
- Very high strain levels attainable (i.e. 1 %, at high fields, or ten times the strain level of PZT before encountering mechanical failure).
- Good linearity at low fields

The listed disadvantages are often overrated or misleading.

- Relatively expensive. (This is true on a per-wafer bases, but if the cost is normalized by the displacement produced, the material is quite competitive.)
- Relatively fragile or brittle. (While it fractures easier than other ceramic actuators such as PZT, it requires no special handling. Further, if loaded in compression it becomes quite tough.)
- A low coercive field. (They do have a lower coercive field, and hence can be more easily depoled. But, as with other PZT ceramics driven at high voltages, this only requires using the appropriate bias or voltage-offset setting on the driver amplifiers.)
- Poor linearity at high fields. (True, but only when used in very-high strain, very-high electric field applications.)

Many of these listed issues are true only in the very-high fields required in the applications that have been largely responsible for supporting its development. These applications require driving the material at voltages near its coercive limit. Under these conditions, any piezoelectric material will appear nonlinear and have high hysteresis. At the lower field strengths used in this study, we shall see that this material has lower hysteresis and better linearity than even PZT-8.

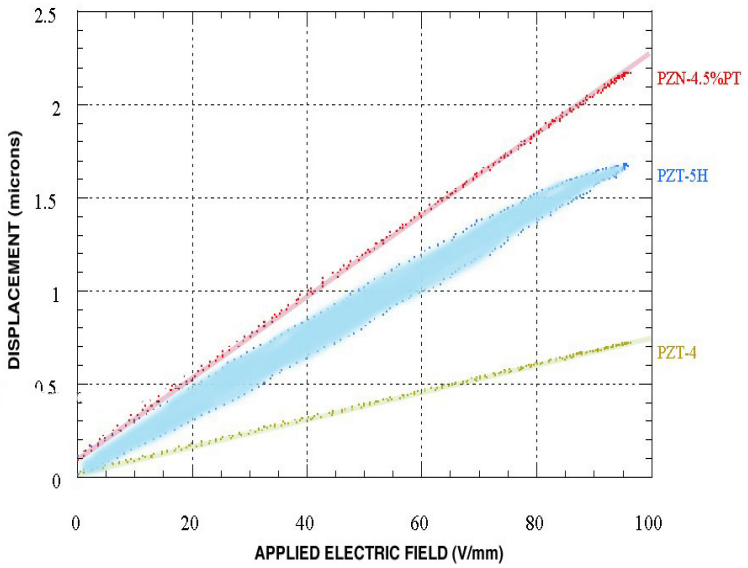

Fig. 24 — Displacement vs. applied field for select transducer materials. (figure from TRS literature)

An interesting set of data is shown in Fig. 24. The displacement produced as a function of electric field strength is shown for three transducer materials: PZT-4, PZT-5, and one particular single-crystal (PMN-PT) formulation. The field strengths shown are those commonly used for moderate-strain applications. As might be expected, the performance of the single-crystal material is significantly higher than either of the other two. However the interesting feature is the apparent linearity and low hysteresis in the single-crystal material, when compared for example to PZT-5 (which exhibits considerable hysteresis).

To examine the potential of using this material in our devices, we compared the characteristics of our previous sensors with predictions for a set fabricated from single-crystal material. The results are shown in Table 5.

Table 5 — Initial comparison of previous and proposed actuators.

	New	**Previous**
Material Type	PMN-PT Single Xtal	PZT-8
Number of wafers	2	10
Thickness	2 mm	8 mm
Effective d_{33}	3300 pm/V	2300 pm/V
Drive Voltage	0 to ± 300	-200 to + 200
Maximum Displacement	0.99 μm	0.92 μm
Cost (material + labor)	$ 1000 + labor	$ 500 - $ 700

The analysis indicates that a two-layer single-crystal stack driven with only 300 V p/p will have the same output as a 10 layer PZT-8 stack driven at 400 V p/p. (Note: had we been willing to use slightly higher drive voltages, a single wafer of the single-crystal material would have sufficed.)When labor is included, the two are comparable in cost, but for the single-crystal material there is an expectation that cost will be further reduced as the material receives wider use.

The attractiveness of single-crystal material in the current application is primarily the smaller thickness of the stack. It also contains fewer glue bonds, which generally introduce loss. (Of little interest here, the two-layer stack would be usable at higher frequency due to its smaller thickness.)

Initial Tests in First Test Article

A trial actuator was fabricated using available single-crystal disks. The unit built is a two-layer stack with perforated metal-shim electrodes. The size of the actuator is compared to that of the previous ITC stacks in Fig. 25. Also shown is a single wafer (disk) of the material. The thickness reduction is seen to be considerable.

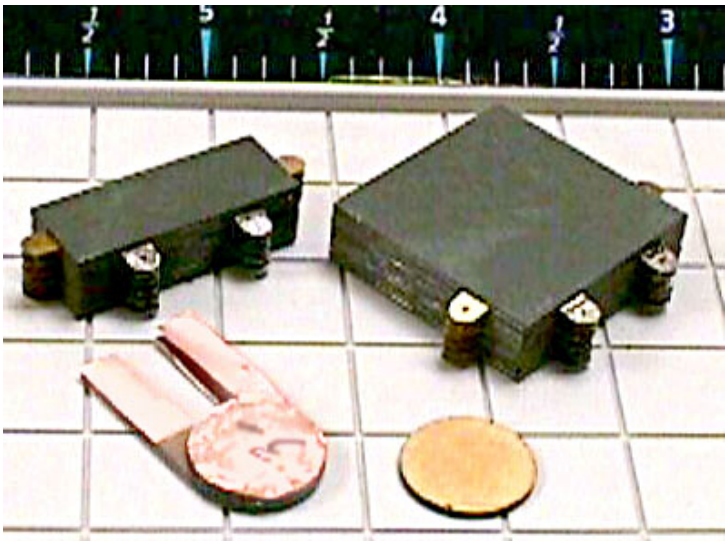

Fig. 25 — Trial single-crystal stack and wafer, (bottom) shown with previous PZT-8 stacks (top)

These single-crystal wafers were borrowed from another study at NRL. The best-matched wafers in the original set were already in use for its intended application. Hence the wafers available for this study were from different material batches and were poorly matched. We began by measuring the properties of all available disk wafers, using our bench-top apparatus and a laboratory fiber optical displacement sensor (PhilTech Model RC12-A2OQR). Variations in the effective d33 ranged from 760 to 1910 pm/V, as shown in Table 6. The stronger and weaker disks were then matched in pairs to provide as near-as-practical matched performance for six units of two-wafer actuator stacks.

Table 6 — Measured piezoelectric constant for available wafers.

Wafer Number	Measured d_{33} (pm/V)	Wafer Number	Measured d_{33} (pm/V)
1	1910	7	760
2	1480	8	1980
3	1300	9	1660
4	900	10	1700
5	1330	11	1390
6	1110	12	1810

Four lateral (x and y axis) actuators and one vertical (z-axis) actuator were fabricated, each containing a single two-wafer stack.

Latter an alternate z-axis actuator was fabricated containing three such stacks. This used some wafers that were originally rejected due to edge-chips. This three-stack actuator used a lateral arrangement to present a greater driving surface area in an attempt at increasing the available force and reducing the importance of precise centering. The installed actuators are shown in Fig. 26.

Fig. 26 — Single-crystal 2-waffer actuator stacks installed on x and y axes (left) and three-stack actuator latter installed on z axis (right)

The results obtained were excellent and highly encouraging. Performance obtained using the single-crystal actuators is at least as good as that found with the previous10-layer PVT-8 stacks. For example, Fig. 27 shows a reduction of 33.3 dB when the system is turned on (relative to the system-off performance which includes only the passive rubber isolator).

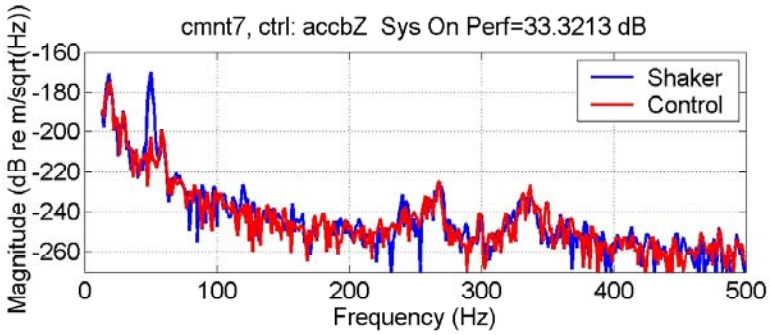

Fig. 27 — Control test with single-crystal actuators in previous device

But the more interesting feature of the data is the very low distortion present. As shown in the above figure, we could detect no evidence of harmonic distortion in the laboratory setups we used. This tentatively places an upper limit on the harmonic distortion value for this material at no greater than 0.02 %, which is our noise floor for this type of measurement. The importance of this low figure is the promise it offers for highly stable, very high performance control in future applications.

The only exceptions to the otherwise excellent performance found with these crystal actuators was due to the unfortunate variations in wafer properties. As previously mentioned, the first test article often had significant levels of cross-axis actuation, contributed largely by the four hangers. The unequal actuation performance of these new actuators appeared to slightly increased this undesirable effect. This

was particularly true when we attempted to use the three-element z-axis actuator (whose use was thereafter suspended).

COMPACT DESIGN AND FABRICATION

Based on the above excellent performance of both the single-crystal actuators and the reduced-complexity device, a more compact version of the previous device was designed. Its design features are similar to that of the previous reduced-complexity device, and so are not repeated here. The principle change is the reduced size, which is afforded by the use of the higher actuation authority of the single-crystal actuators.

The principle features of this compact design are:

- Size is limited largely by size of rubber isolators and ease of handling.
- Full Three-Axes isolation and actuation.
- Less than 25 mm (1 inch) thick and 51 mm (2 inches) square.
- Usable at all orientation angles

Note that thickness can be further reduced to less than 19 mm (0.75 inches) if some inert material positioning standoffs are reduced or removed.

Actuator Fabrication

Actuator wafers were commercially purchased to NRL size specifications from TRS Ceramics, who developed their procedure under ONR and DARPA contracts. This is the same supplier of the disks used previously. (Similar material is also commercially available from H. C. Materials Corporation (HCMC), which is also an ONR contractor and DARPA consortium member.) Fig. 28 shows a photograph of these new wafers as compared to the previous PZT-8 stacks.

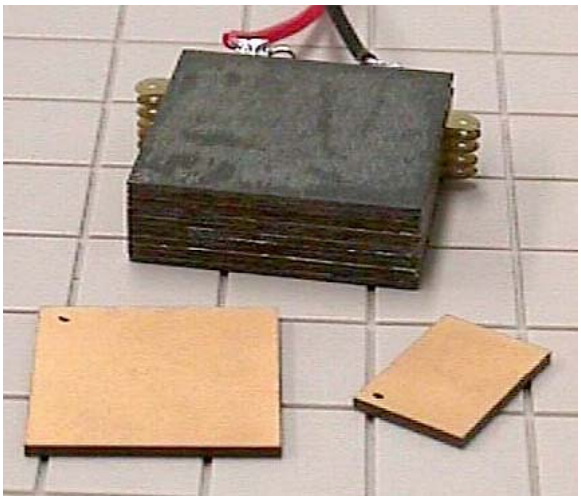

Fig. 28 — New single-crystal wafers, compared to the previous PZT-8 stack

The wafers are 1mm thick, composed of PMN-32 %PT. The plates are oriented <001> relative to the large faces and poled through the thickness. They were obtained with a Cr/Au 500/2000 Å sputtered metal coating. At the time of purchase, the cost was $2.50 per square mm of surface area. The sizes ordered were 20×20 and 10×15 mm.

Table 7 — Properties (nominal) listed for Single Crystal PMN-PT

Property	Value from TRS		HCMC literature
	Literature	Delivered (ave)	
K_{33}^T	5000	6760	5500 - 6800
d_{33} (pC/N)	2000	1966	2000 - 3000
Y_{33} (GPa)	-	-	16 - 20
E_c (V/mm)	-	-	250
k_{33}	0.91	-	0.91
Tan(δ)	-	0.007	0.008

The nominal property values listed in the literature for these actuator types are given in Table 7. They include the relative dielectric constant K^T, the piezoelectric constant d_{33}, the Young's Modulus Y_{33}, the depolarization field limit EC, and the damping tan(δ). The average values of these properties for the delivered wafers are also included. The piezoelectric constant and capacitance for the individual delivered wafers are given in Table 8. The consistency in the properties of these actuators is very good, and comparable to that typically obtained with conventional PZT ceramics. The data tabulated is from the manufacturer's measurements. A spot check by NRL using different equipment confirmed these results.

Table 8 — Properties of delivered wafers (Manufacturer's data).

Size series	Part #	Thickness (mm)	Capacitance (pF)	d_{33} (pC/N)
20 x 20 mm	1	1.012	24250	1926
	2	1.023	25260	1947
	3	0.995	25270	2119
	4	1.000	24400	1948
10 x 15 mm	1	1.014	8244	1959
	2	1.005	9573	1513
	3	1.008	8655	2117
	4	1.004	8911	1772
	5	1.000	8758	1931
	6	1.018	8864	1957
	7	1.016	8562	1985
	8	1.007	9108	2185
	9	1.009	8462	1977
	10	1.011	9067	1970
	11	1.003	8422	1976
	12	1.010	9069	2184

The fabrication of the new actuator stacks from two wafers of these crystals involved preparation of fabrication fixtures and development of an assembly procedure. Two Teflon gluing fixtures were machined (one for each actuator size). Each contains holes for five pins, located appropriately to align the two fixture halves and various parts, as shown in Fig. 29.

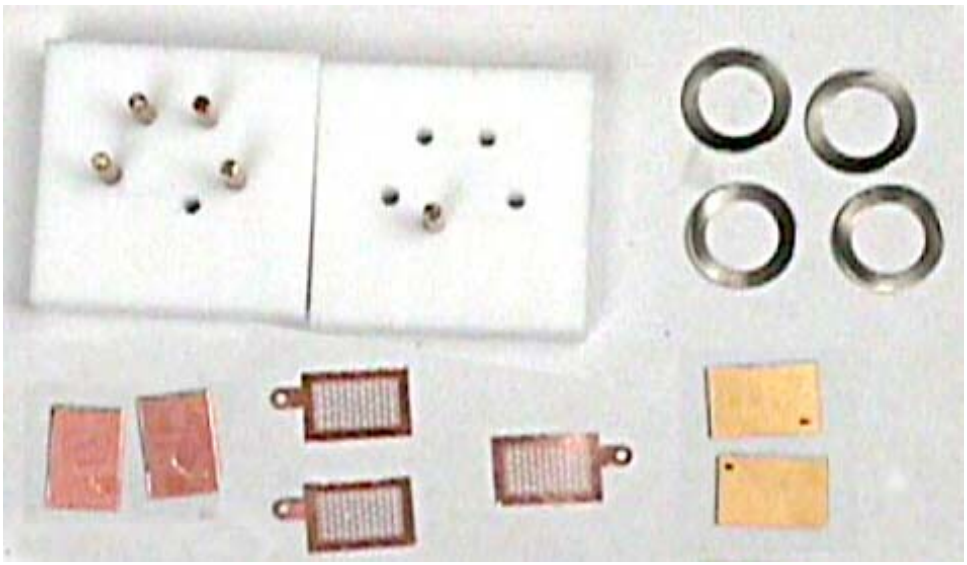

Fig. 29 — Components for fabricating single-crystal stack. Bottom from left are two cover plates, three perforated metal electrodes, and two crystal wafers. Top is the gluing fixture and disk springs

The assembly procedure had a number of steps. The first was to insert a 0.081 mm copper-plated GRP cover, and apply a very small quantity of low-viscosity adhesive (Master Bond type EP-30 epoxy). A perforated electrode shim was added next, followed by the first wafer, another shim, the second wafer, another shim, and the final GRP cover. Fig. 30 shows a photograph of the actuator assembly. Between each of the above layers, a very small amount of additional adhesive was added. The entire fixture was then squeezed in a machinist vise, using four disc springs (4.65 lb each, size 5/8 × 3/8 × .013 inch, McMaster Part #9716K82) to limit and hold the compressive force applied to nominally 18 lb. This was found to produce very thin, uniform glue bonds.

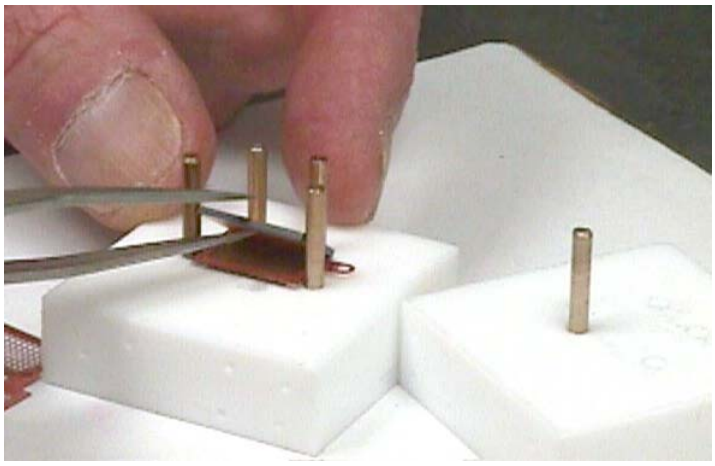

Fig. 30 - Assembly of the actuator stack

The perforated electrode shim was designed to match the wafer dimensions. It was designed at NRL, and custom-fabricated by Lancaster Metals Science Corp., (Lancaster PA). It is formed from 1 mm thick soft copper. The perforated holes in the central region of the metal sheets let the epoxy penetrate. This yielded a good glue bond between the transducer wafers, with enough metal-to-surface bite to form a

good electrical connection. This is a common practice in transducer stack fabrication. The two different sizes of electrodes needed were formed in one tooling operation, and were separated along a perforated line (using a razor) on delivery. Each electrode contained two connection tabs, one of which would typically be removed (depending on the orientation needed).

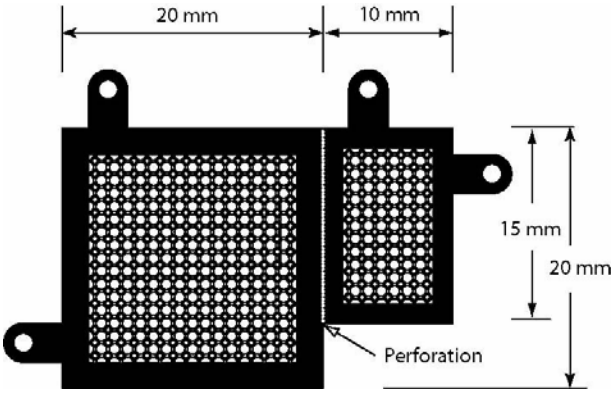

Fig. 31 — Perforated combined electrode. Cut along perforated line shown to form one of each size needed

The final actuators fabricated are shown in Fig. 32. As shown, they are nominally 3.8 mm thick. Approximately half of this thickness is contributed by the PC board covers, which serve only as mechanical protection.

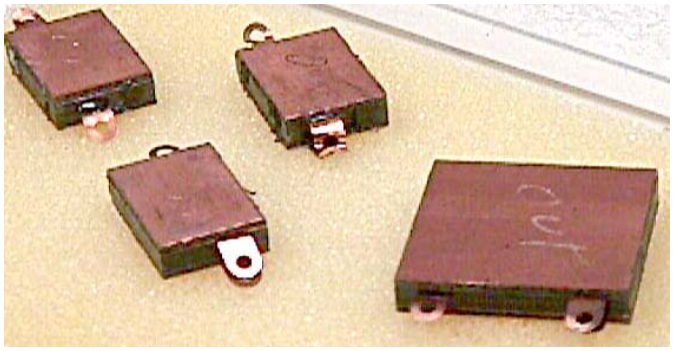

Fig. 32 — Actuators fabricated

The actuators were not configured identically. One of each x-y pair was made with the positive electrode surface (Y1) on the inside, while the other had the negative electrode (Y2) on the inside. These were then wired as a push-pull pair, as shown in Fig. 33, where the outside electrodes were connected in common (YC).

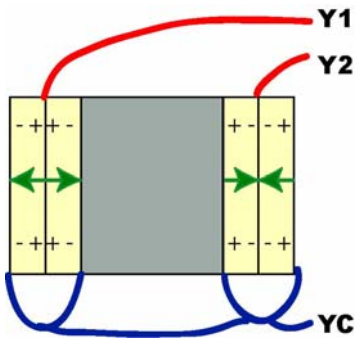

Fig. 33 — Actuator push-pull wiring (Y-axis example)

This new wiring arrangement accommodates both unbiased operation at low drive voltages, and biased operation at high drive voltages, as explained shortly. The PC board connections are shown in Fig. 34.

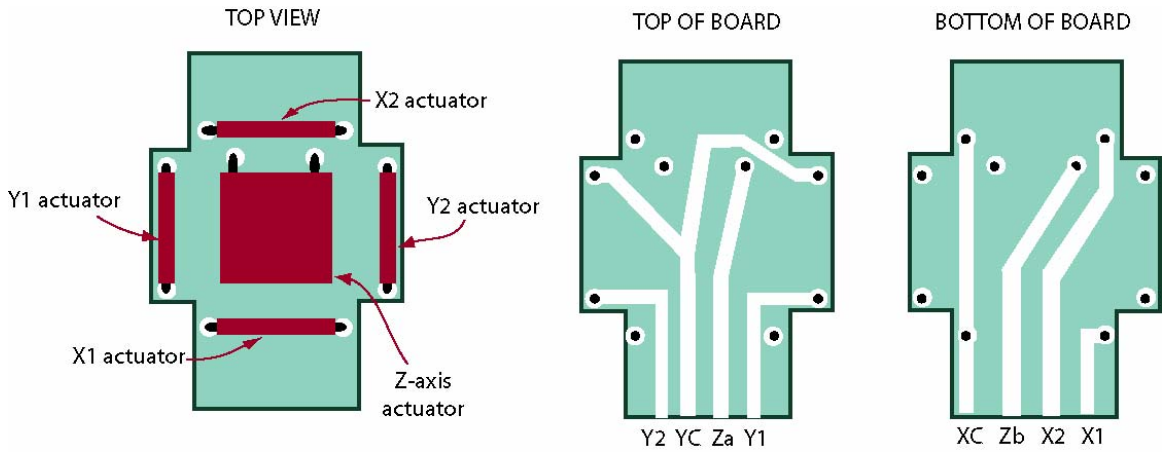

Fig. 34 — PC board wire connections

With this new wiring arrangement, for low voltage AC signals, i.e. less than 250 V p/p (peak-to-peak), Y1 can be connected to Y2. Using YC as their common, the two actuators of the pair can be driven in parallel with a single power. Similarly X1 and X2 would be shorted with XC as their common.

In principle, the displacement produced should be approximately independent of frequency at low frequencies. As a quality-assurance test, the actuators were temporarily bonded to a rigid backing, and their displacement output measured with the optical probe. The drive voltage used was 160 V p/p (80 V negative and positive). The result is shown in Fig. 35, where the displacement uniformity is seen to be quite good. (The small variations at the highest frequencies shown are simply mechanical artifacts of the temporary mounting arrangement.)

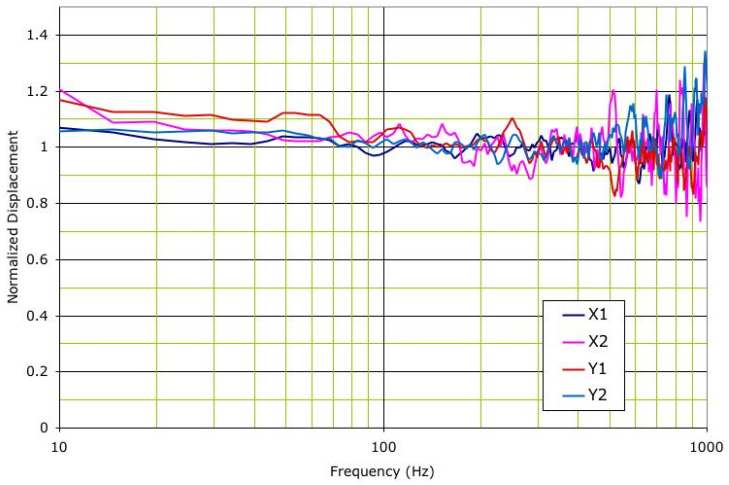

Fig. 35 — Actuator displacement frequency dependence

For higher AC drive levels, the driver pair must be separately driven. The AC signal applied to each actuator stack would be identical, but the DC bias would be different. The bias (or DC offset) is needed since ceramics can be depolarized by strong electric fields applied with polarity opposite to the original poling voltage. Values for recommended positive and negative drive voltages for common ceramics were given in Table 7 of the previous report. For the single crystal material used here, E_c is only 250 V/mm. The usual recommendation is not to exceed one-half this field strength in the negative direction. In the positive direction, fields as high as 2 kV/mm can be used with reasonably good linearity. Hence the recommended voltage limits and a typical bias level are given in Table 9. The bias example given is for delivering a 500V p/p AC signal, which is somewhat higher than the 300 V p/p needed for this test.

Table 9 — Voltage limit recommendations for wafers used.

	Y1	Y2
V(-) max	-125 v	-2000V
V(+) max	+2000 v	+125
Bias for 500 V p/p AC signal	+200	-200

Note that the above electrical drive signals can be obtained using either two separate drive amplifiers, or just one AC drive amplifier with auxiliary circuitry to apply the DC bias (DC power supplies with blocking capacitors and/or AC isolation transformers).

Rubber Isolators

The passive isolators are rubber pads similar to those used in the previous device. Once again, the spring constant of the total passive isolation assembly should be nominally 30,000 N/m in all three directions, and the same type of rubber is used.

The dimensions used differ somewhat from those of the previous device. The four lateral (corner) isolators were chosen to be as small as practical. These were fabricated from a single layer of rubber material, 1.5 mm thick. The vertical isolators were chosen to be somewhat larger, so as to cover the face

of the transducer elements. To obtain approximately the same shear spring constant, the thickness had to increase. This was obtained by bonding two layers of rubber.

Table 10 — Rubber isolators used in the Compact device.

Isolator	Area	Thickness	Spring Constant		
axis	(mm x mm)	(mm)	Shear (N/m)	Long. (N/m)	Total System
X, Y (Lateral)	10 x 10	1.5	8.5 x103	200 x103	24.8 x103
Z (Vertical)	10 x 15	3.0	6.4 x103	69 x103	30.3 x103

The resulting dimensions and properties for the individual pads and total system are given in Table 10. As before, the longitudinal spring constants are seen to be much larger than the shear and do not contribute appreciable compliance.

Assembly

The parts for the device are shown in Fig. 36. Because this device is intended to be reproduced, the machinist drawings are included here in the Appendix.

The z-axis actuator is shown attached to the central piston, which in this case is machined from a block of Plexiglas. A lower printed circuit (PC) board is also attached to this block, with the two z-axis wires passing through the block and soldered to the z-axis actuator. This central section is shown just resting in the lower stage, which has the lateral-shear rubber isolators adhered to pillars on the four corners. The x and y axis actuators are shown in the lower portion of the figure with the z-axis shear rubber isolators already attached to them.

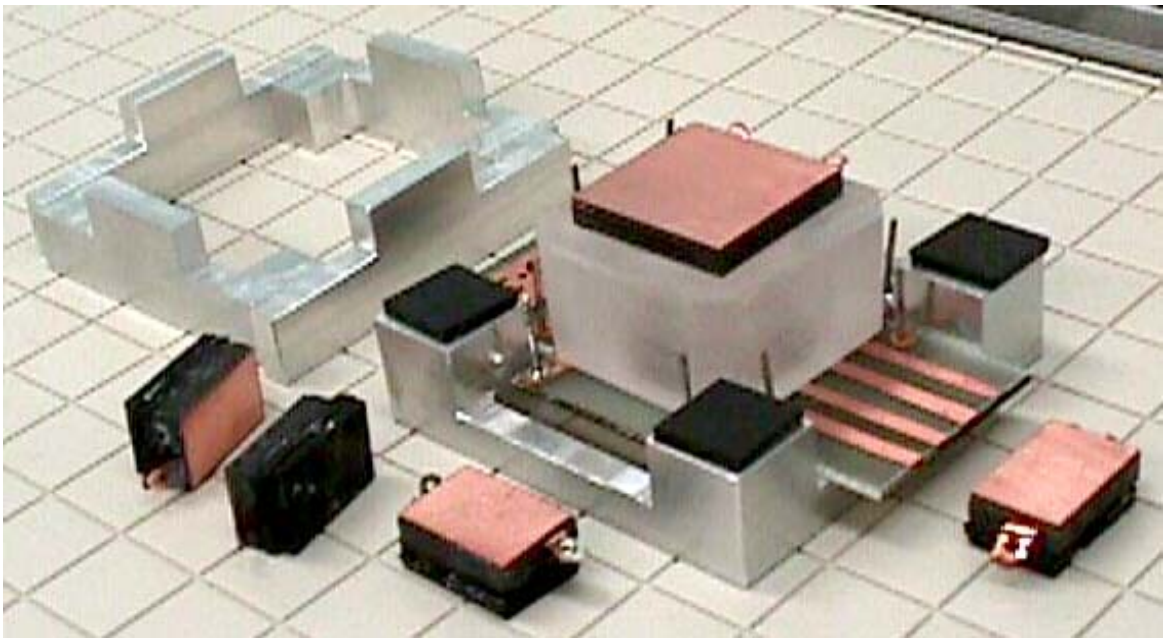

Fig. 36 — Parts assembly for the Compact device

The next step in the fabrication is to put adhesive (Loctite #404) on both surfaces of these actuator-isolator assemblies, and adhere the actuator side to the central block. The central piston then resembles that previous shown in Fig. 20. While the adhesive is still fluid, the four sections of the upper frame are then assembled around them (using four screws), with the rubber isolator side becoming adhered to this upper frame. The actuators are then soldered to the wires projecting from the lower PC board, and finally this upper unit is then adhered to the rubber isolators on the pillars of the lower unit.

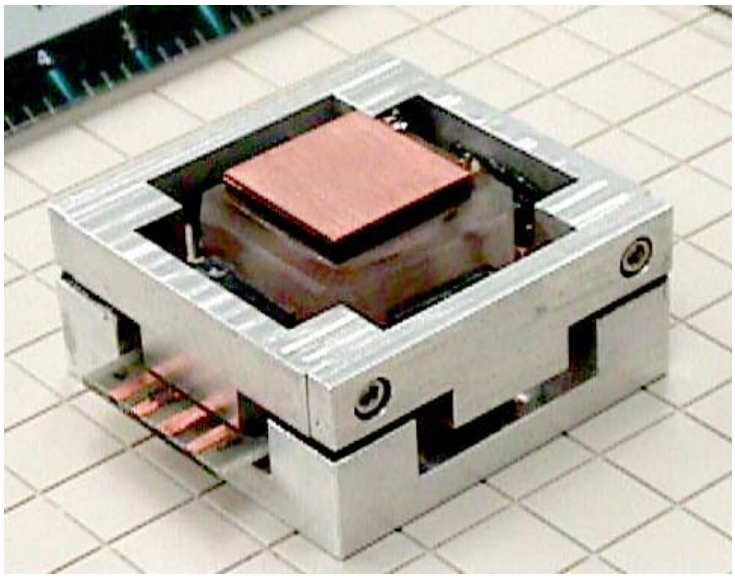

Fig. 37 — Compact device. (Background grid is 0.5 inch spacing.)

The resulting device is shown in Fig. 37. A bottom view showing the PC board wiring connections appears in Fig. 38.

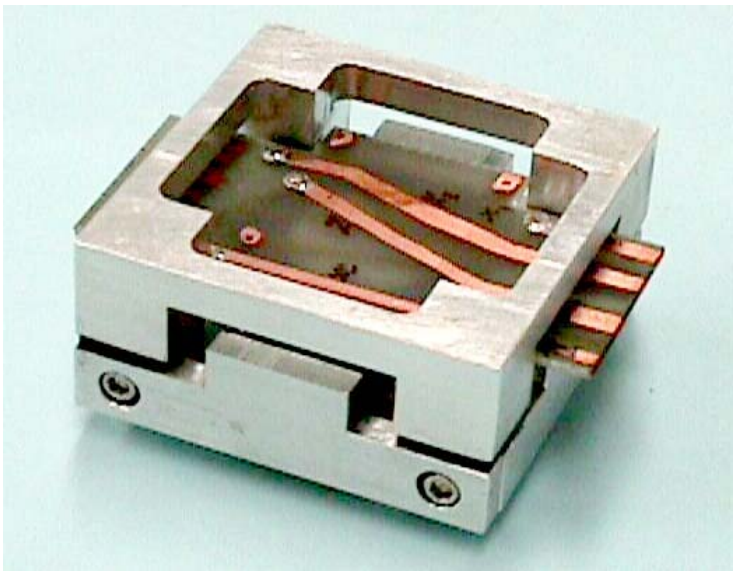

Fig. 38 — Bottom view of device

Test Results

Experiments were conducted with the compact device at the Laboratory for Structural Acoustics, Naval Research Laboratory in May-August 2004. The experimental goals were to evaluate the performance and reliability of the 3-dimensional compact device in a single mount configuration. Single-tone (50 Hz) experiments were performed as well as a full multi-tone demonstration with as many as 8 harmonics of 50 Hz.

The experimental configuration is the same as that used in the previous experiments (see Fig. 15). Three Wilcoxon F3 electromechanical shakers and an above mount mass are used to simulate vibrating machinery. Their combined above mount mass is 7.7 kg. In the single tone experiments, all three shakers are driven with a 50 Hz sinusoid at a magnitude of approximately 60 dB re $\mu g / \sqrt{Hz}$. This level is about 10 dB below the specified level. Recall that, in addition to the shaker disturbance, the piezoceramic actuators must also have this same drive authority. A DC bias circuit for the single crystal material was not available for these tests, limiting the AC drive level of the actuator. However, the results indicate that the full 70 dB re $\mu g / \sqrt{Hz}$ can be achieved with this device when a bias circuit is implemented.

The fundamental resonances of the system were measured, and they are listed in the Table 11. The above mount mass and base plate move in-phase with each other in the first resonance and out-of-phase in the second resonance.

Table 11 — Measured system resonance frequencies.

	Resonance 1	Resonance 2
X	9.6 Hz	18.5 Hz
Y	9.1 Hz	18.0 Hz
Z	11.3 Hz	21.1 Hz

The feedforward ‘system-on’ configuration for the z-axis is illustrated in Fig. 39. This configuration has been illustrated for the z-axis only, but the same control configuration is repeated for the x-axis and y-axis. The ‘system-on’ scheme consists of three separate Single Input-Single Output (SISO) loops that are all run simultaneously. The loops are independent of each other and are not fully interconnected through the processor. Each loop consists of its own error sensor, LMS algorithm, FIR filter, power amplifier and a single crystal piezoceramic actuator. In this configuration, the x-axis actuator minimizes the x-axis base accelerometer, the y-axis actuator minimizes the y-axis base accelerometer and the z-axis actuator minimizes the z-axis base accelerometer.

The FIR control filter is formed via the use an adaptive Least Mean Squared (LMS) algorithm. The two inputs to the LMS algorithm are the error signal and an electrical reference that is correlated with the disturbance (F3 shaker). In the single-tone experiments, the LMS algorithm adapts eight weights in the FIR filter while the output drives a power amplifier and the appropriate actuator. Higher order FIR filters will be required for the multi-tone experiments. The weights adapt until convergence, and the error signal is minimized in a least mean squared sense.

The number of weights is optimized through a set of experiments. This experimental process involves starting with a low number weights and gradually increasing the number until no additional performance is found in the reduction of the error sensor. Theoretically, only two weights are required to control the gain and phase at a single frequency, but in the presents of system noise and system (plant) variations more weights are usually required.

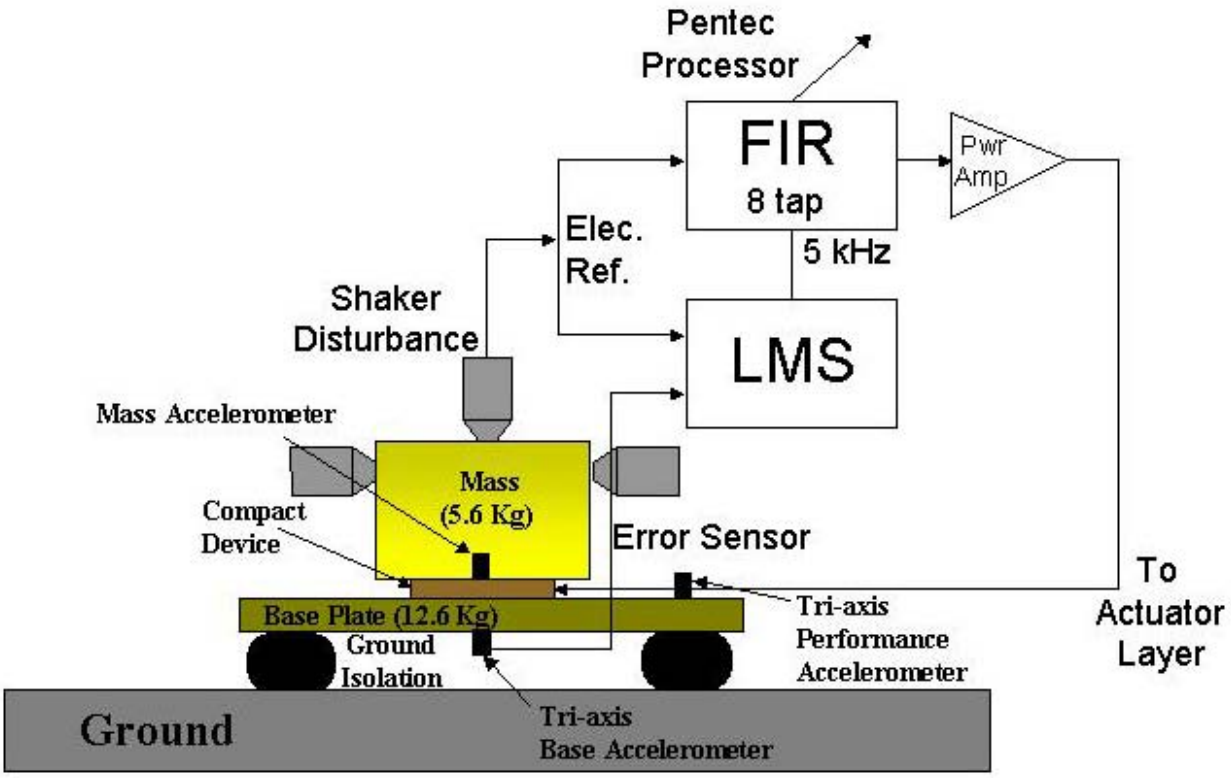

Fig. 39 — Controller Configuration.

The error sensors (tri-axis base accelerometers) are minimized simultaneously during the control experiments. Usually very large reductions are found at the error sensors since they are minimized directly. The main performance metric, however, is evaluated downstream from the compact device at the tri-axial performance accelerometers. The single-tone results are summarized in the bar graphs shown in Figs. 40 and 41, and the detailed frequency domain results can be found in Appendix B.

The error sensor reductions (Fig. 40) indicate that the system-off (passive) reductions are in the 16 to 18 dB range. An additional 24 to 41 dB reduction is due to the system-on actuation of the compact device, yielding a total reduction of 41 to 58 dB at the error sensor. The downstream performance results are shown in Fig. 41. Passive reduction of 13 to 19 dB was found with system-on performance in the 18 to 23 dB range. The total performance at the downstream location was found to be 31 to 41 dB for all three axes. It is also important to note that these excellent control results were achieved with very low levels (< 60 dB) of harmonic distortion enhancements from the single crystal actuators (also see Appendix B).

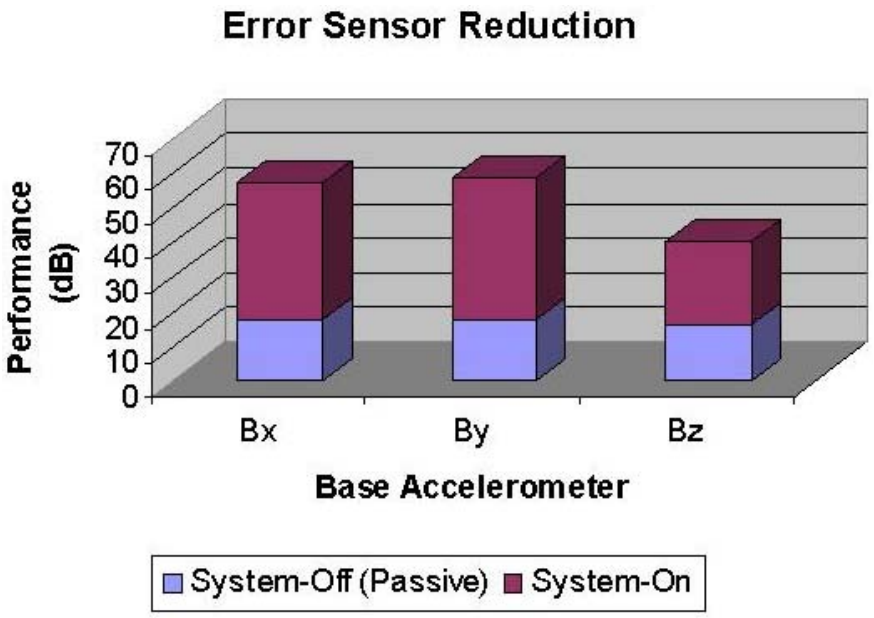

Fig. 40 — Error Sensor Reduction.

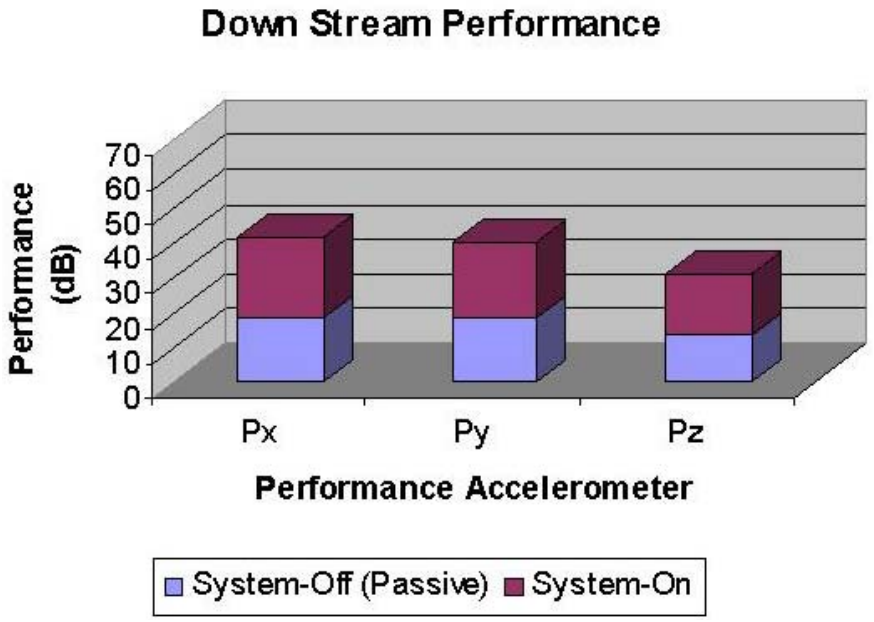

Fig. 41 — Downstream Performance.

With good performance results in the single tone experiments, the next step was to work with multi-tone harmonic inputs. The first experiments were performed with a two-tone input (50 Hz and the first harmonic at 100 Hz). The summarized results from these experiments are shown in Figs. 42 and 43, and the detailed frequency response curves may be found in Appendix C. These two-tone experiments led to a full multi-tone demonstration with as many as 8 significant harmonics. These multi-tone results are

summarized per sensor and harmonic frequency in Figs. 44 through 49 with the detailed frequency response curves in Appendix D.

In the two-tone experiments, the reduction in the error sensor (Fig. 42) indicates that the passive reduction averaged 15.5 dB (50 Hz) and 26.1 dB (100 Hz). The combined system-off (passive) and system-on reduction averaged 53.7 dB (50 Hz) and 41.5 dB (100 Hz). The required order of the optimal LMS-adapted FIR filter remained fairly low, consisting of 24 taps for each of the three filters in these experiments. The results of the two-tone experiment at the downstream accelerometer (primary performance metric) are summarized in Fig. 43. The average performance at this location due to passive alone is 23.5 dB (50 Hz) and 32.6 dB (100 Hz). The combined average performance from both system-off (passive) and system-on is 44.6 dB (50 Hz) and 43.0 dB (100 Hz).

The performance results show approximately the same level of total performance for each peak with a higher contribution from the system-on component at 50 Hz than at 100 Hz. Recall that the effectiveness of the passive system quickly increases at frequencies beyond the low frequency resonances of the isolator. These resonances are all below 21 Hz for this system in all directions. The passive isolation effect will be even more dramatic with the higher frequency harmonics in the multi-tone experiments.

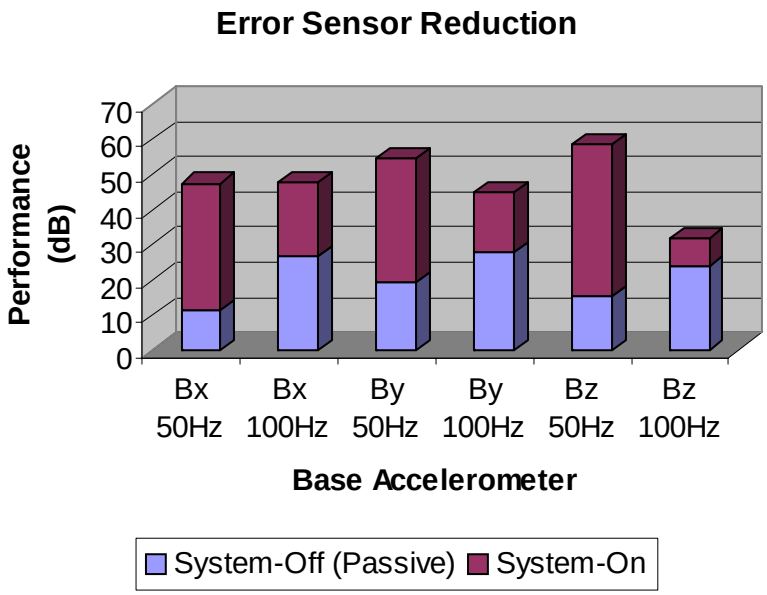

Fig. 42 — Error Sensor Reduction, Two-Tone.

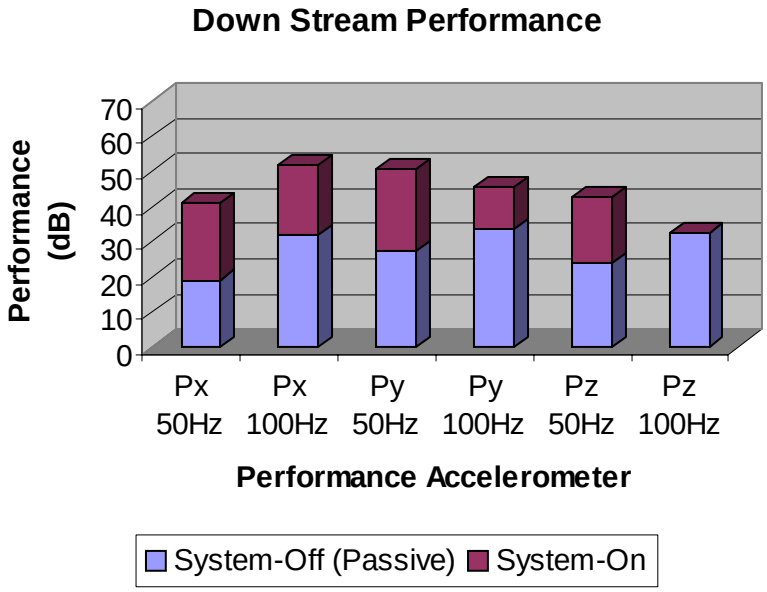

Fig. 43 — Downstream Performance, Two-Tone.

The results of the full multi-tone (up to 8 harmonics) demonstration are summarized in Figs. 44 through 46 in terms of the error sensor reduction and in Figs. 47 through 49 for the downstream performance metric. Observing the detailed frequency response curves in Appendix D, note that it was difficult to control the level of all the harmonic peaks when so many are present. (i.e. The harmonic peaks do not all start at the same level relative to the noise floor.) These variations must be taken into account when forming conclusions about the performance results. The combined reduction levels in the bar graphs appear higher at the lower frequency harmonics, but this is simply due to the fact that the initial levels (no isolation) are generally lower at the higher harmonics.

These results show that the hybrid device is combining the passive and 'system-on' components in an effective manner. The system-on component of the hybrid device significantly enhances the performance at the lower frequency harmonics, where the passive system is least effective. The passive component of the hybrid system takes hold of the overall performance beyond approximately the second harmonic (150 Hz). These higher harmonics are practically reduced to the noise floor by the passive isolation, requiring little effort from the system-on component of the device.

In achieving these results, the optimal FIR filters required 64 taps. This filter order is still considered relatively simple and can easily be implement in low cost microprocessors. An optimal design might involve a system-on component that focuses on the first 2-3 harmonics and lets the passive component handle the others, reducing the 64-weight FIR filter order.

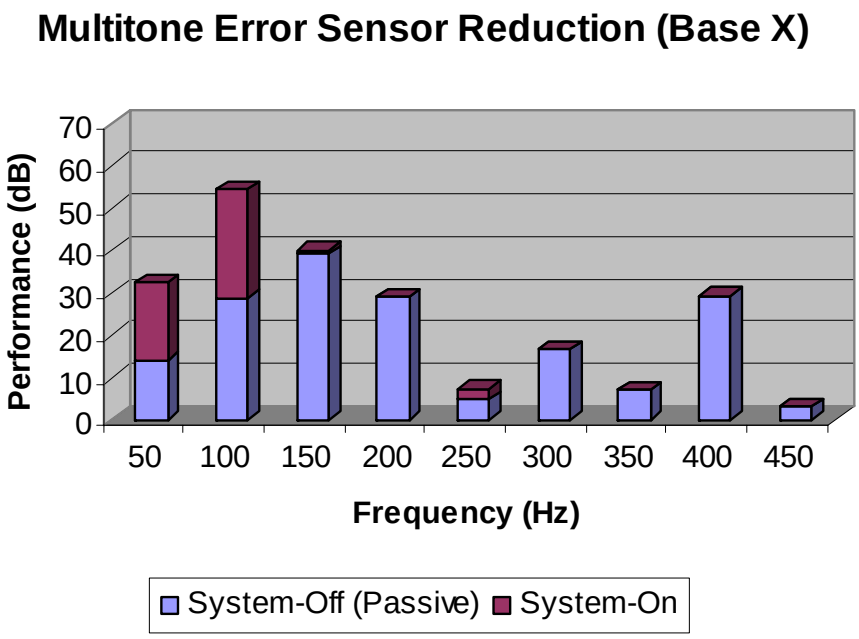

Fig. 44 — X Error Sensor Reduction, Multitone.

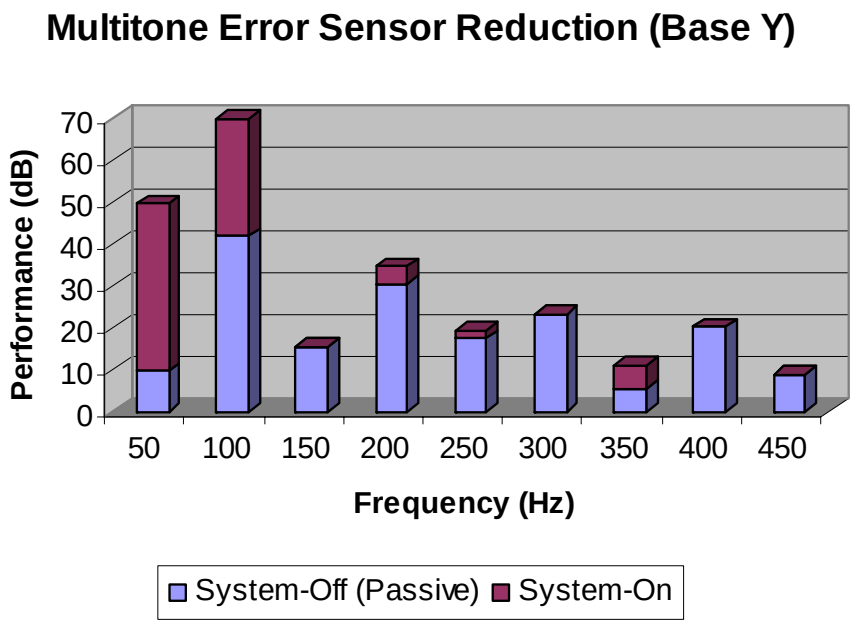

Fig. 45 — Y Error Sensor Reduction, Multitone.

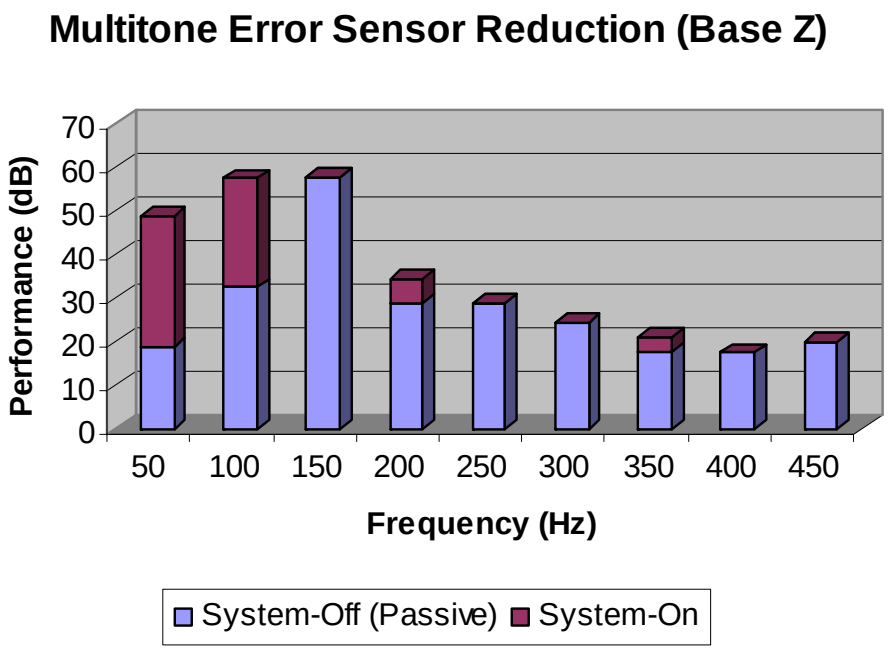

Fig. 46 — Z Error Sensor Reduction, Multitone.

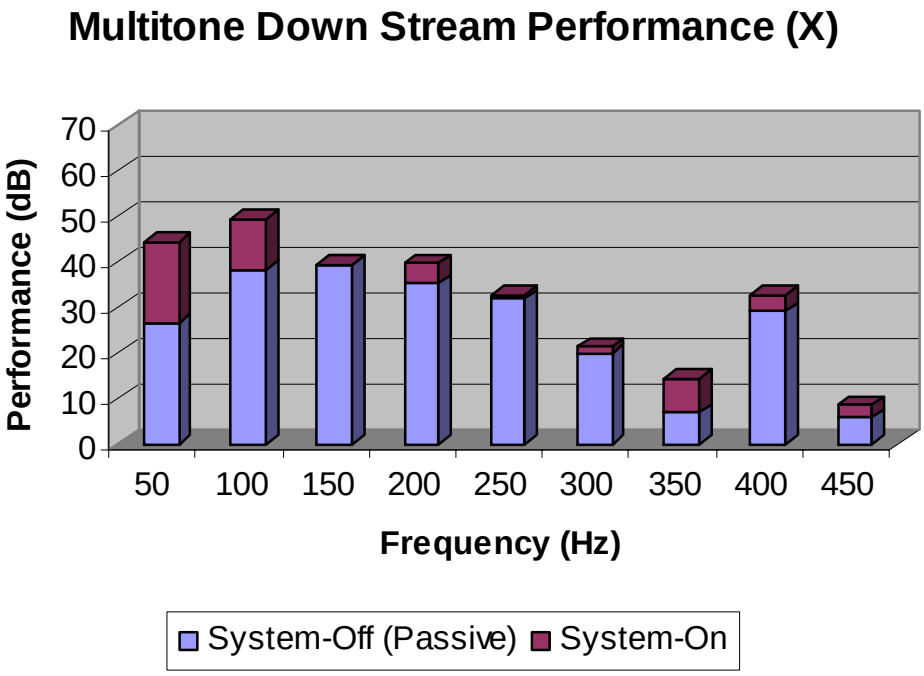

Fig. 47 — X Downstream Performance, Multitone.

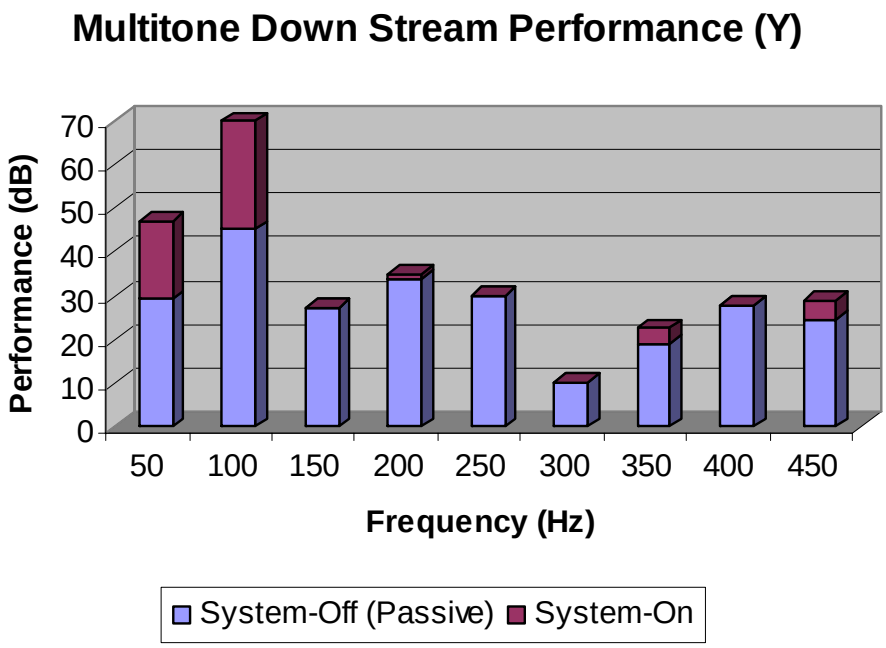

Fig. 48 — Y Downstream Performance, Multitone.

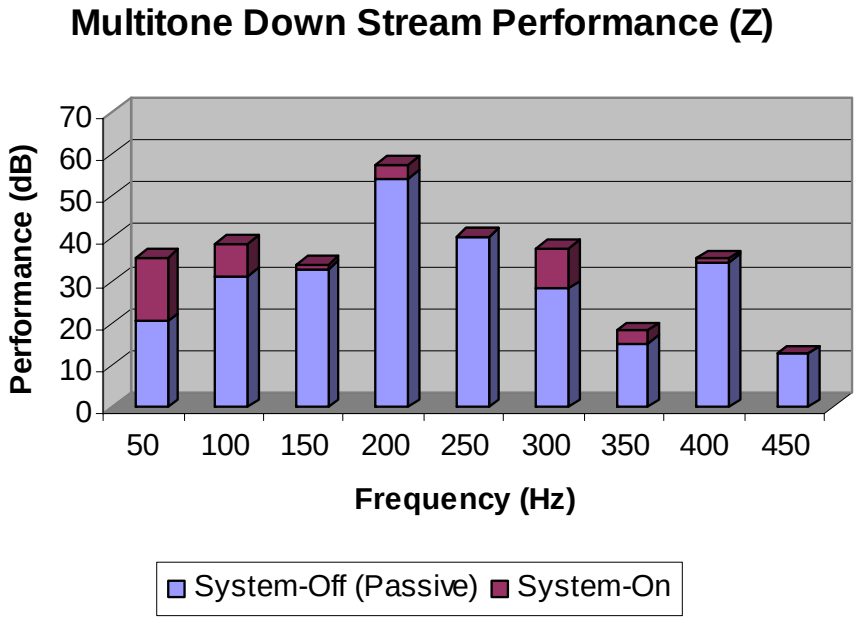

Fig. 49 — Z Downstream Performance, Multitone.

Discussion

While still a laboratory device, the fabrication costs are not low. The cost of reproducing this compact device is estimated in Table 12. These costs assume a few units (i.e. four) will be fabricated

simultaneously, and there is no parts allowance included for breakage or spares. It does not include the associated components such as accelerometers and control electronics.

Table 12 — Cost estimate per device (2004)

	Single Element	**2-wafer stack**
Ceramic (single crystal)	**$2500**	**$5000**
Machining (metal and plastic)	4 hrs	
Assembly - Transducers	4 hrs	
Assembly - mechanical	4 hrs	
QC testing (actuator performance)	4 hrs	

Two actuator configurations are considered in this table. The unit fabricated and evaluated contained actuator stacks consisting of two wafers. This was found to provide sufficient displacement even when driven at low voltages without bias. However for multiple units, it becomes cost-effective to use single-wafer actuators and higher drive voltages. For example, the bias need to drive the actuators with 500 V p/p AC signals was previously considered in Table 9. Implementing this drive condition requires only one DC power supply with ± 200 V outputs, and appropriate blocking capacitors and inductors in line with each actuator of each device supplied. Hence the additional electronics needed to apply the dc bias to multiple devices should be inexpensive.

Obviously the cost can decrease as experience is gained with this new technology, and as multiple units are fabricated. The cost of the single-crystal actuators is currently $250 per cm^2, but this price is expected to decrease by half if there is sufficient demand.

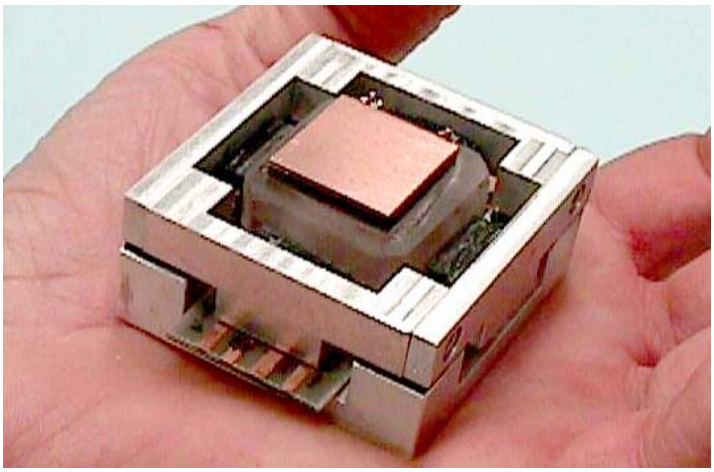

Fig. 50 — Compact Tri-axial Hybrid Device.

CONCLUSIONS

Three instrumented devices were described.

- A **Fully Instrumented** 3-axis device, containing 3-axis force and acceleration sensing.

- A **Reduced Complexity** 3-axis device without lateral force sensors for a much simpler mechanical construction.
- A small **Compact** 3-axis device which uses single-crystal piezoelectric actuators to greatly reduce device size (Fig. 50).

The principle accomplishments of this study are:

- The first demonstration of simultaneous 3-axes vibration reduction using a hybrid device.
- The first device delivering robust, reproducible, high-performance (~30 - 45 dB) in 3-axis downstream vibration reduction of multiple tones.
- The first device that is sufficiently well-behaved and highly linear that it can achieve this high performance level using just a base acceleration minimization.
- The first use of single-crystal piezoelectric actuator stacks in a successful vibration isolation application.
- The first demonstration of an efficient ultra-low distortion piezoelectric actuator.
- The first such device of sufficiently small-size and simple-fabrication that it offers potential for being used in practical applications.

REFERENCES

1. R. Corsaro, B. Houston, P. Herdic, “Hybrid Actuator for Single Axis Control”NRL/MR/7130-03-866 (submitted for external review, Feb 03)

2. R. Corsaro, P. Herdic, J. Klunder, B. Houston “Tri-axial hybrid vibration isolator” submitted for external review 9/29/03. Approved for release Jan 04. Currently undergoing NRL preparation as patent disclosure.

Appendix A

FABRICATION DRAWINGS

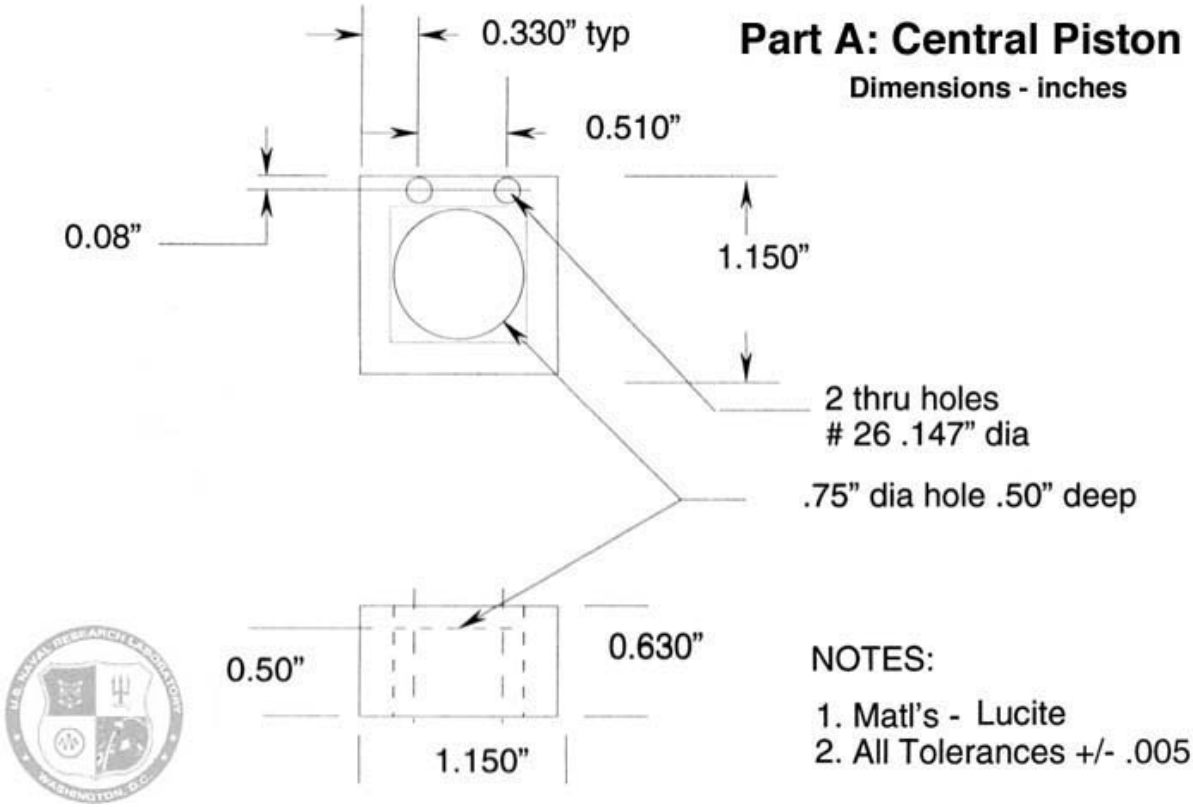

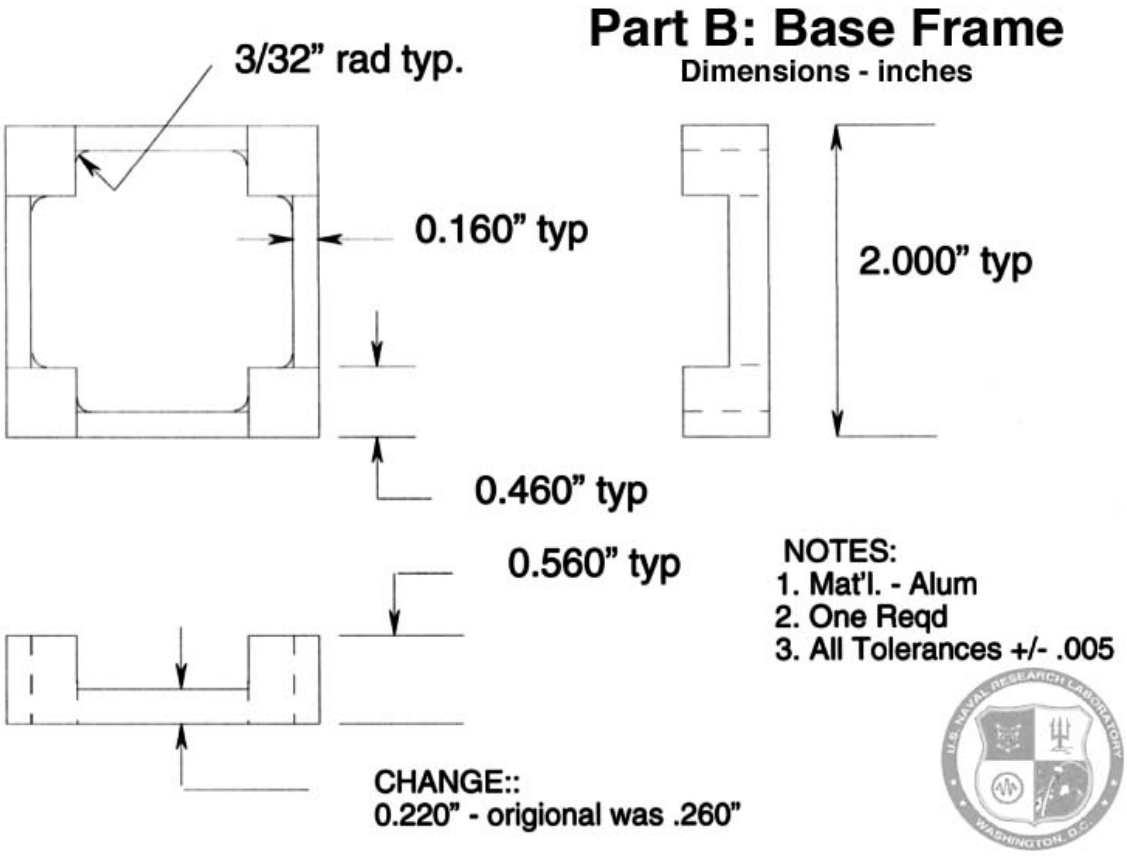
Part B: Base Frame
Dimensions - inches
3/32" rad typ.
0.160" typ
2.000" typ
0.460" typ
0.560" typ
NOTES:
1. Mat'l. - Alum
2. One Reqd
3. All Tolerances +/- .005
CHANGE::
0.220" - origional was .260"

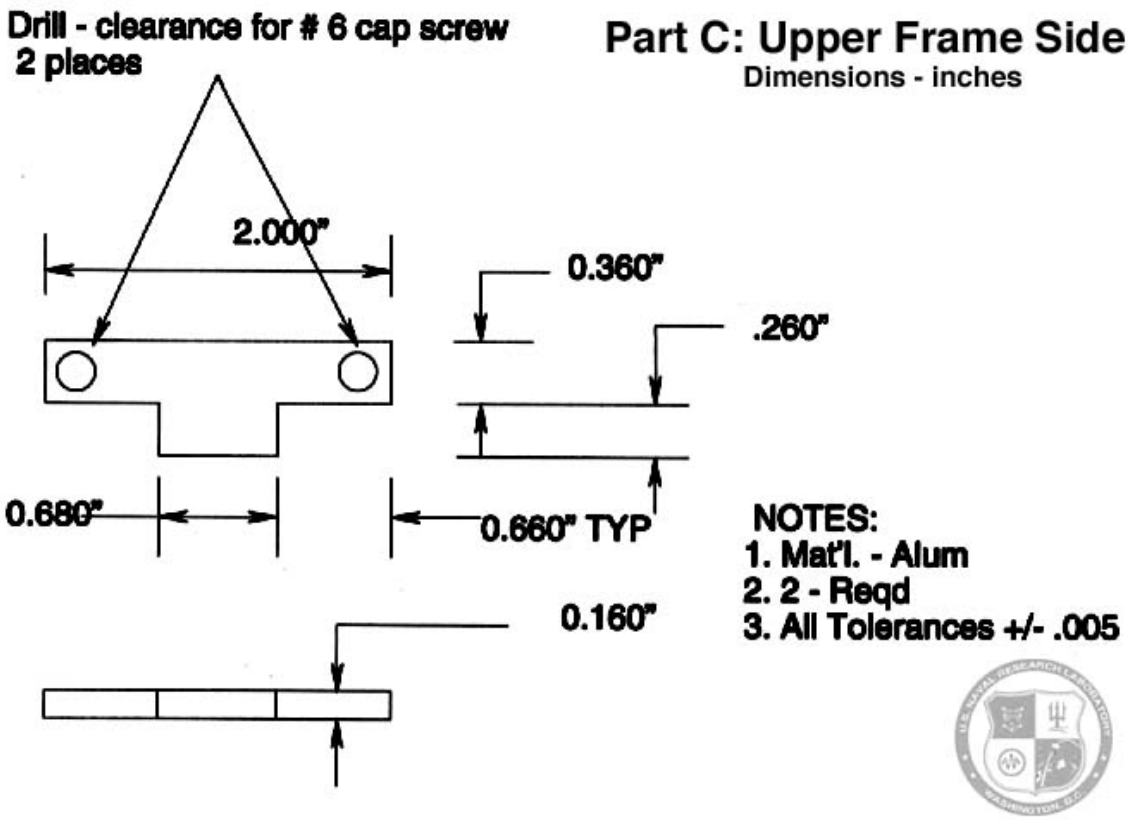
Drill - clearance for # 6 cap screw
2 places
Part C: Upper Frame Side 1
Dimensions - inches
2.000"
0.360"
.260"
0.680"
0.660" TYP
0.160"
NOTES:
1. Mat'l. - Alum
2. 2 - Reqd
3. All Tolerances +/- .005

Part D: Upper Frame Side 2

Dimensions - inches

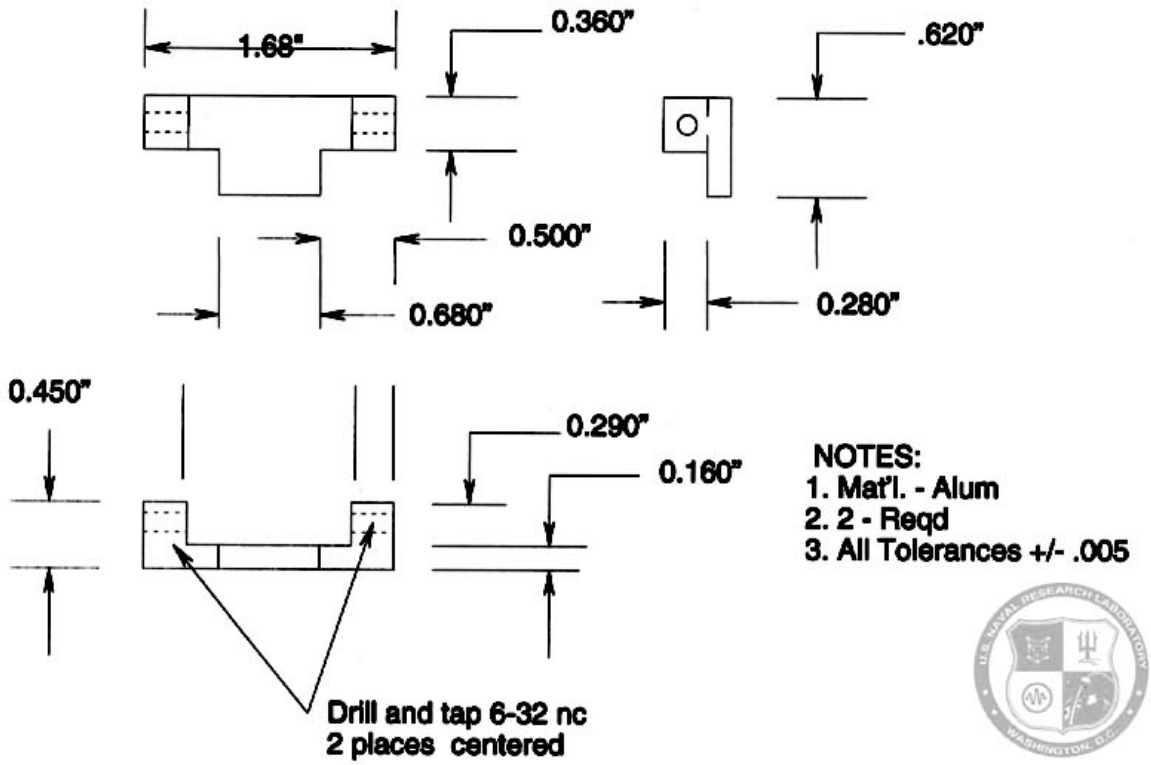

NOTES:
1. Mat'l. - Alum
2. 2 - Reqd
3. All Tolerances +/- .005

Appendix B:

COMPACT DEVICE DETAILED SINGLE-TONE RESULTS

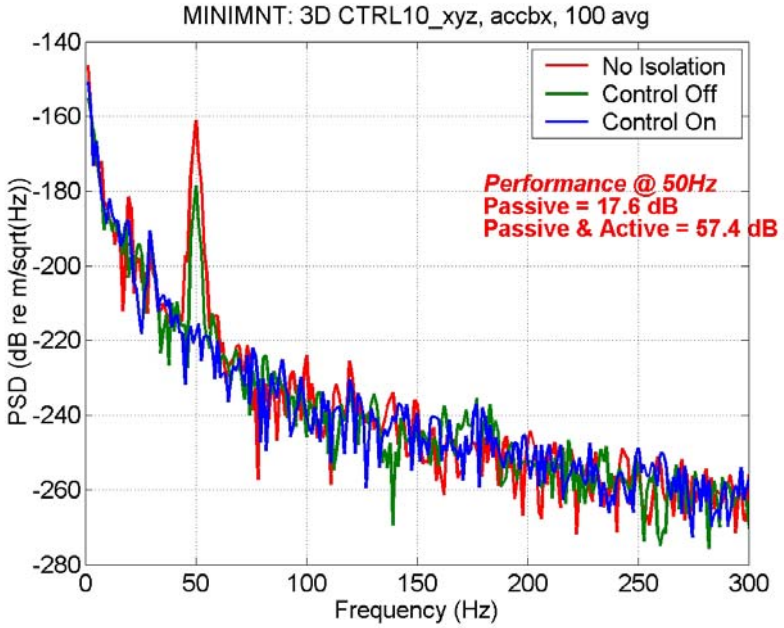

Fig. B1 — No-isolation/Control-off/Control-on frequency response display of **base** accelerometer in **x-direction** due to single tone excitation.

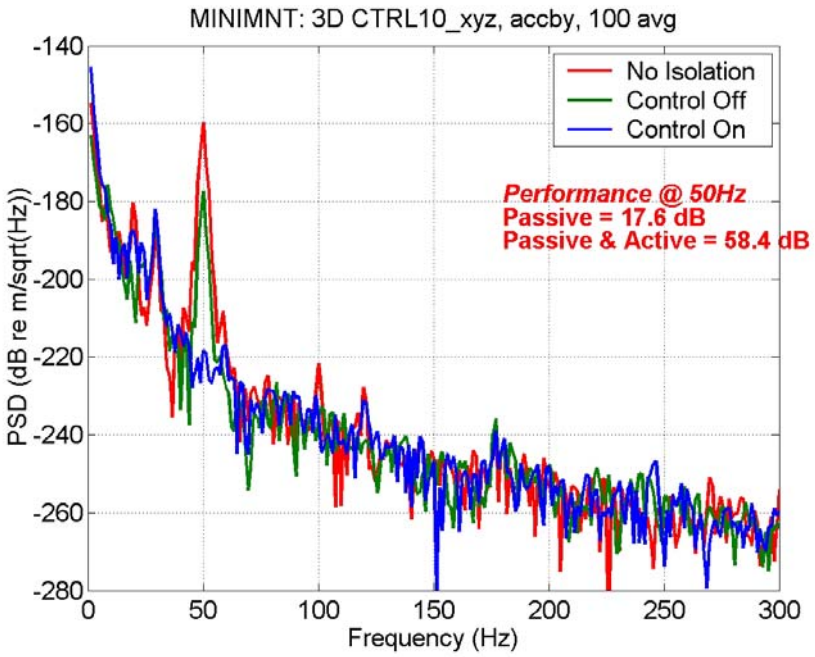

Fig. B2 — No-isolation/Control-off/Control-on frequency response display of **base** accelerometer in **y-direction** due to single tone excitation.

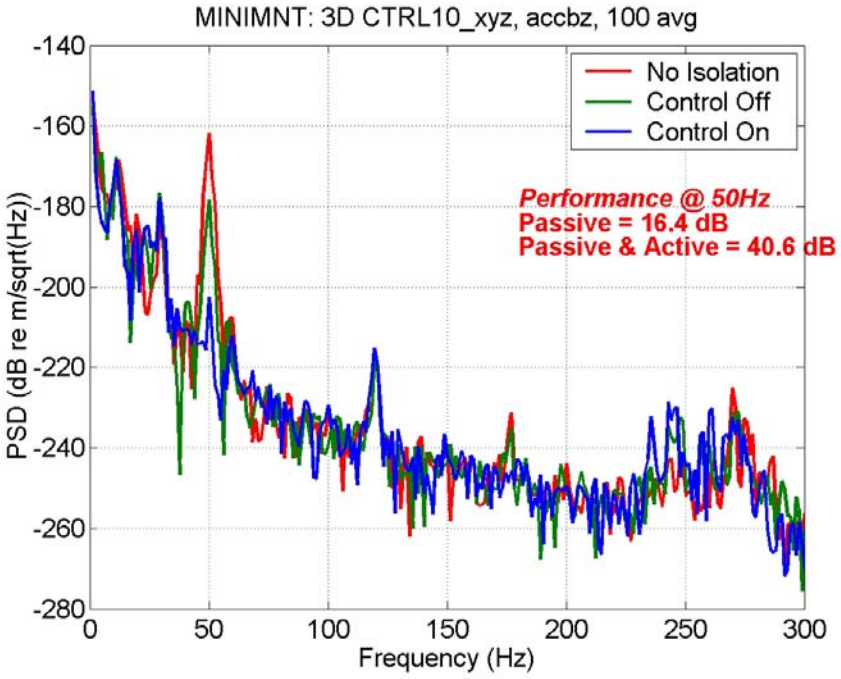

Fig. B3 — No-isolation/Control-off/Control-on frequency response display of **base** accelerometer in **z-direction** due to single tone excitation.

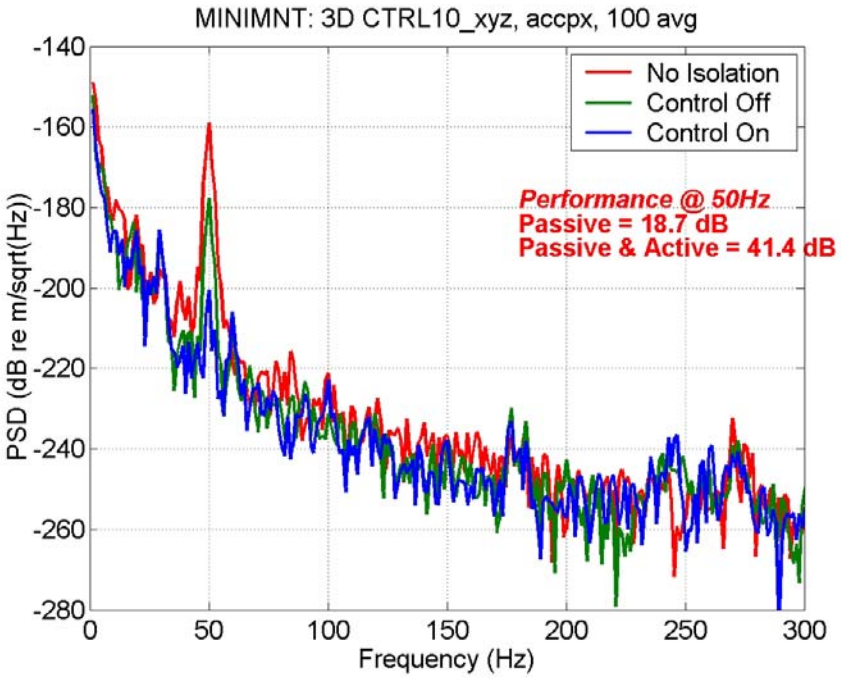

Fig. B4 — No-isolation/Control-off/Control-on frequency response display of **performance** accelerometer in **x-direction** due to single tone excitation.

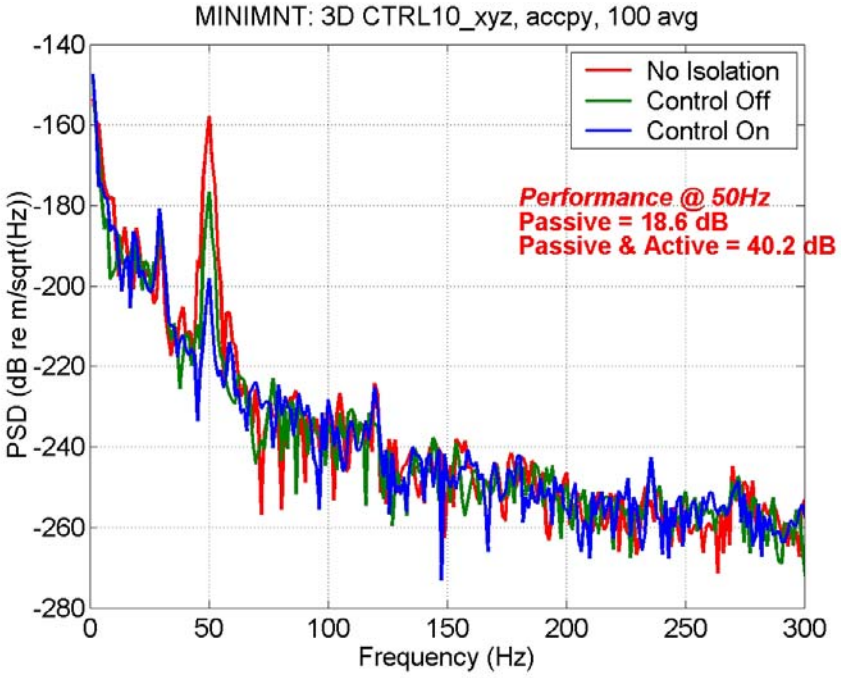

Fig. B5 — No-isolation/Control-off/Control-on frequency response display of **performance** accelerometer in **y-direction** due to single tone excitation.

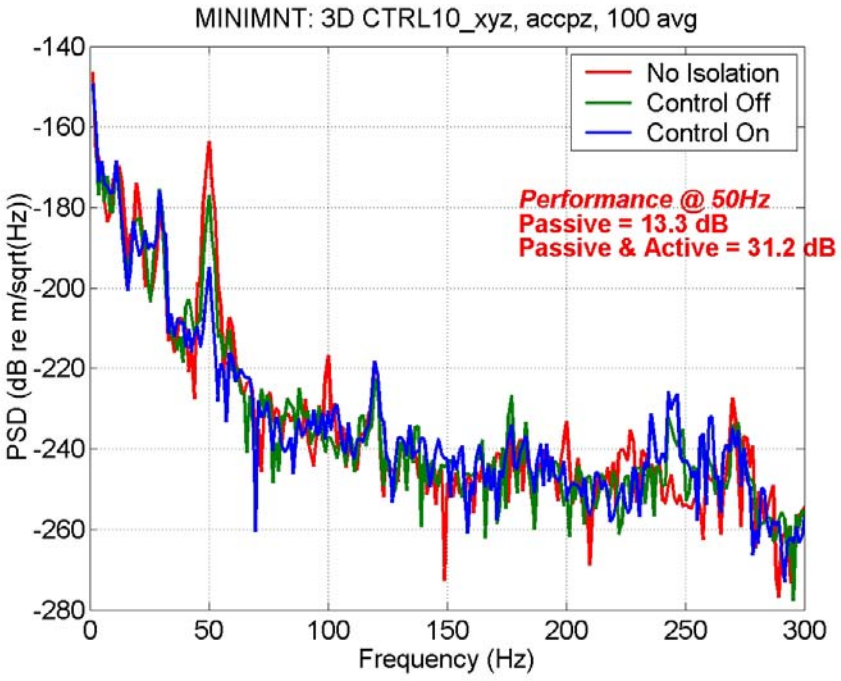

Fig. B6 — No-isolation/Control-off/Control-on frequency response display of **performance** accelerometer in **y-direction** due to single tone excitation.

Appendix C

COMPACT DEVICE DETAILED TWO-TONE RESULTS

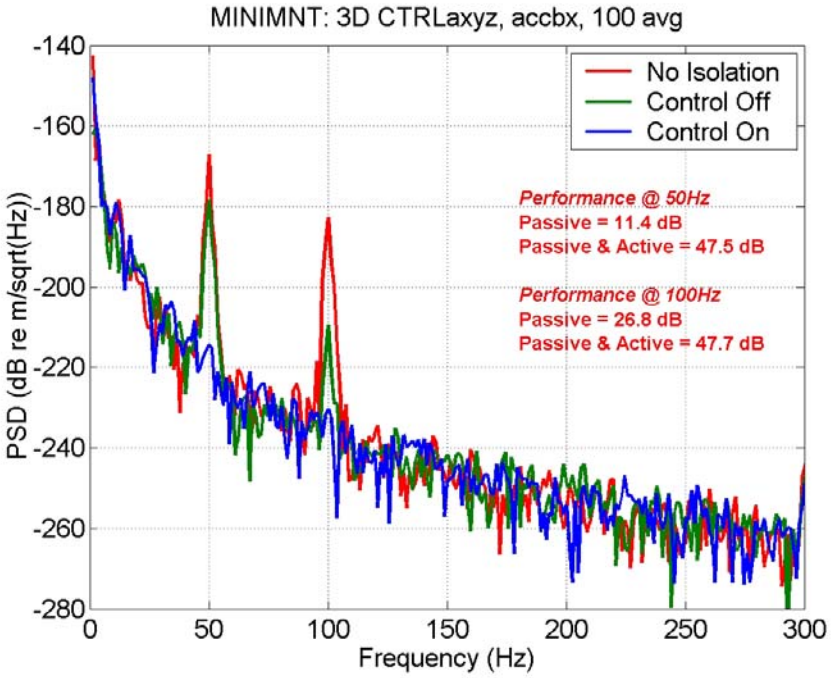

Fig. C1 — No-isolation/System-off/system-on frequency response display of **base** accelerometer in **x-direction** due to two tone excitation.

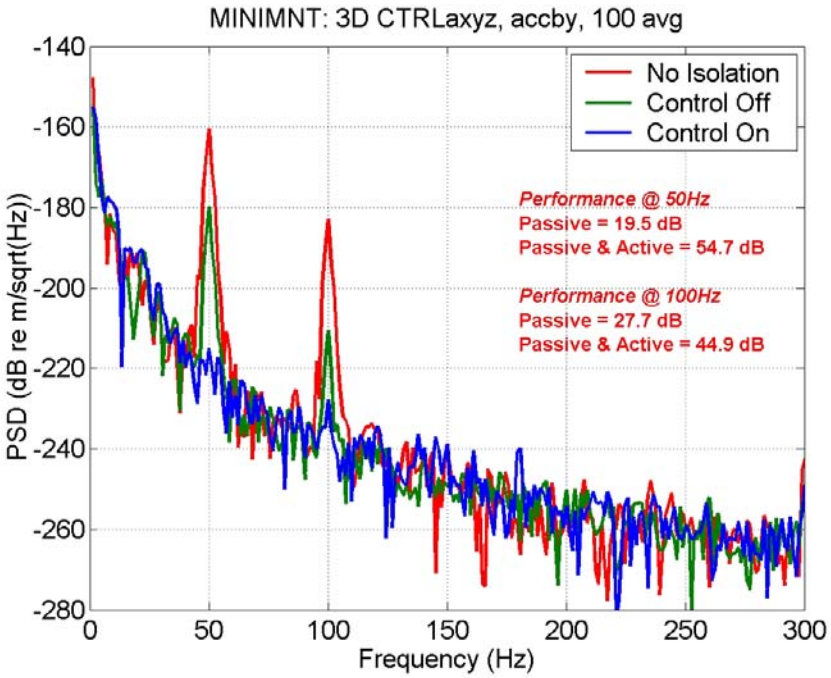

Fig. C2 — No-isolation/Control-off/Control-on frequency response display of **base** accelerometer in **y-direction** due to two tone excitation.

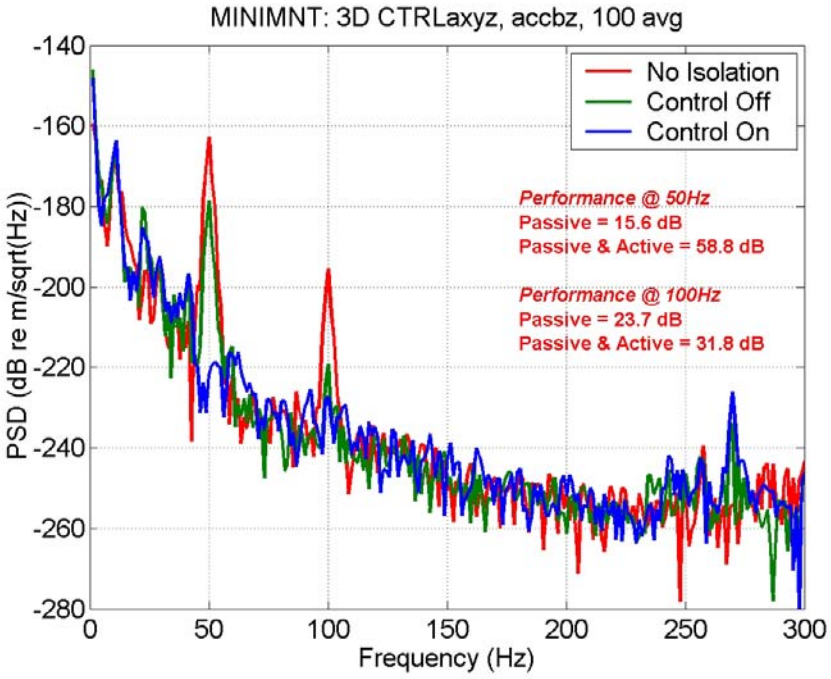

Fig. C3 — No-isolation/Control-off/Control-on frequency response display of **base** accelerometer in **z-direction** due to two tone excitation.

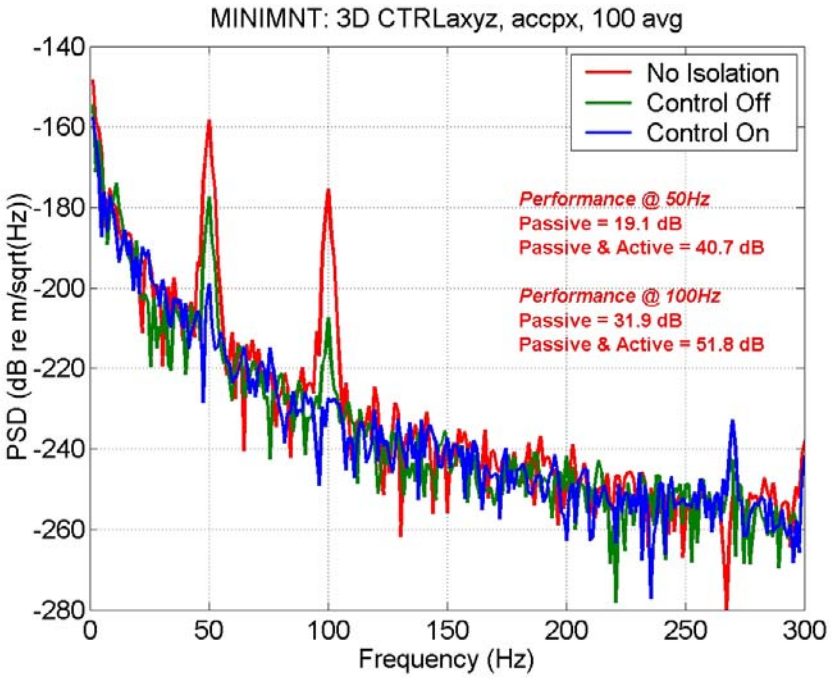

Fig. C4 — No-isolation/Control-off/Control-on frequency response display of **performance** accelerometer in **x-direction** due to two tone excitation.

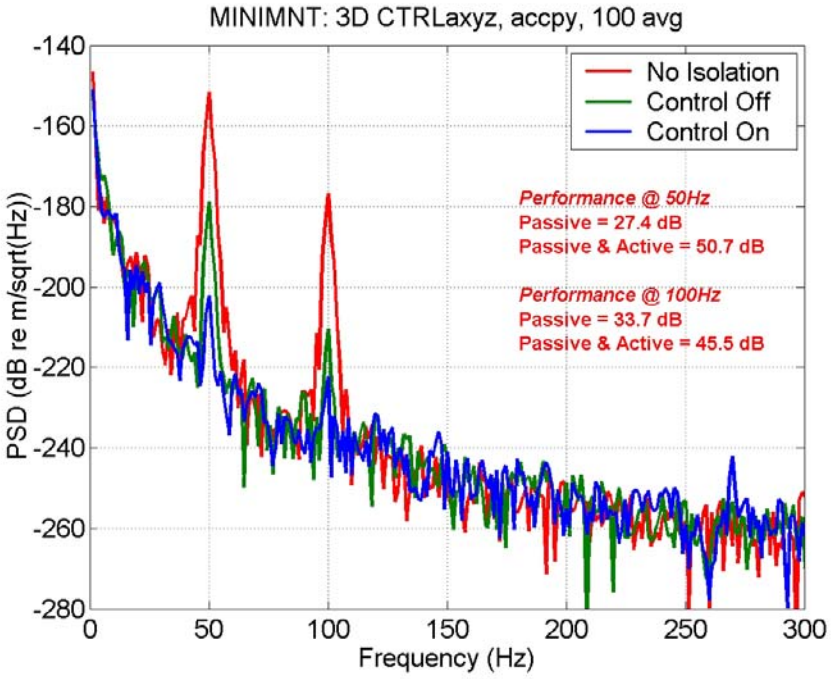

Fig. C5 — No-isolation/Control-off/Control-on frequency response display of **performance** accelerometer in **y-direction** due to two tone excitation.

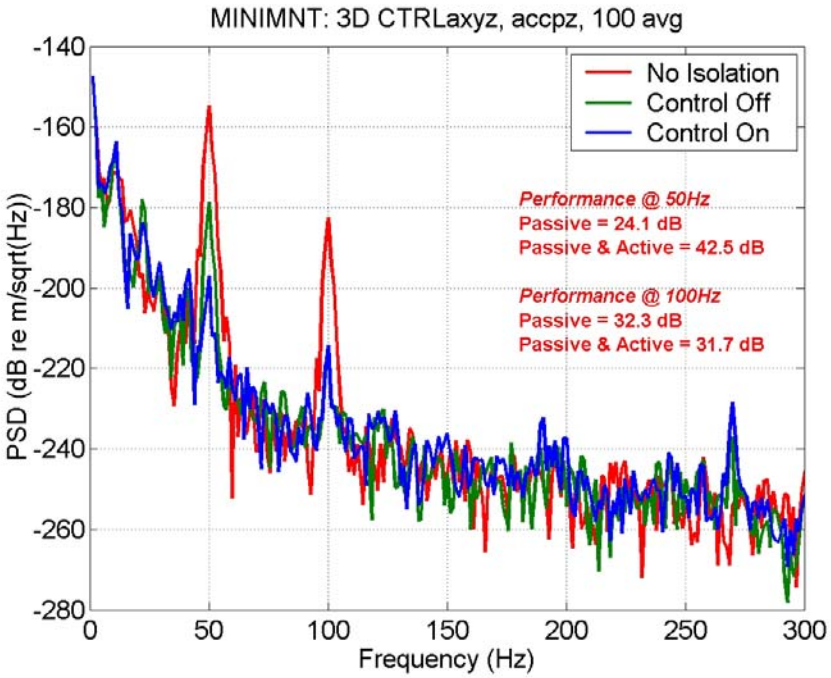

Fig. C6 — No-isolation/Control-off/Control-on frequency response display of **performance** accelerometer in **y-direction** due to two tone excitation.

Appendix D

COMPACT DEVICE DETAILED MULTITONE RESULTS

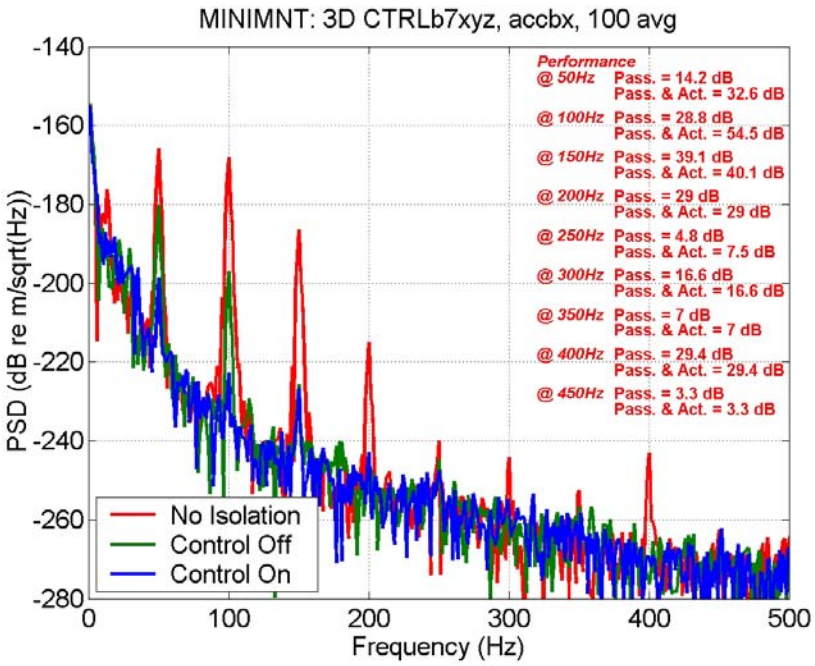

Fig. D1 — No-isolation/Control-off/Control-on frequency response display of **base** accelerometer in **x-direction** due to multitone excitation.

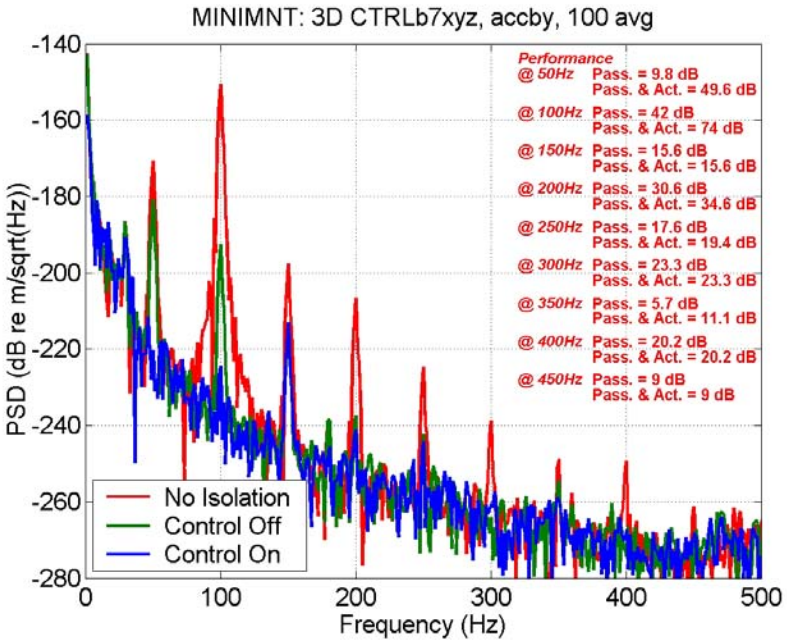

Fig. D2 — No-isolation/Control-off/Control-on frequency response display of **base** accelerometer in **y-direction** due to multitone excitation.

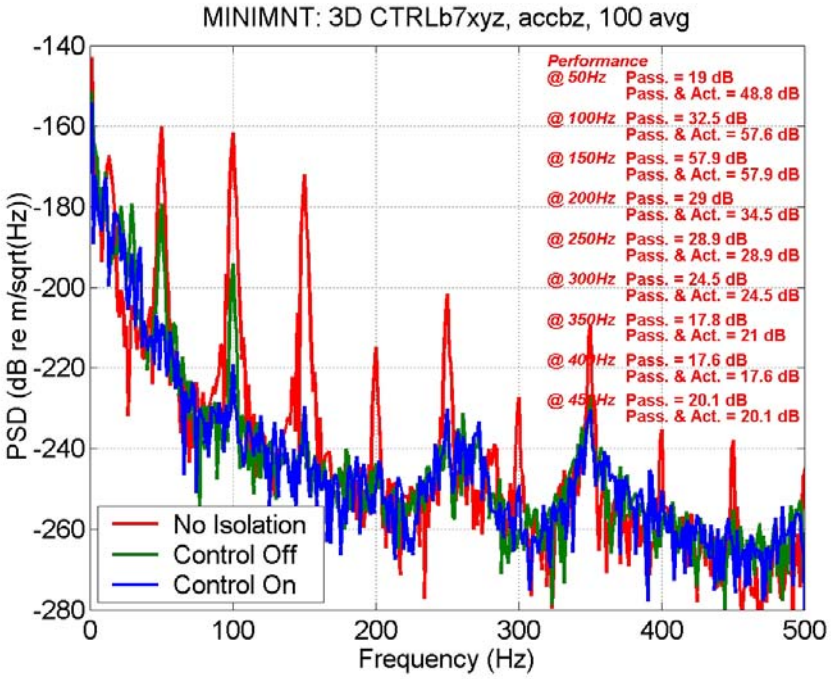

Fig. D3 — No-isolation/Control-off/Control-on frequency response display of **base** accelerometer in **z-direction** due to multitone excitation.

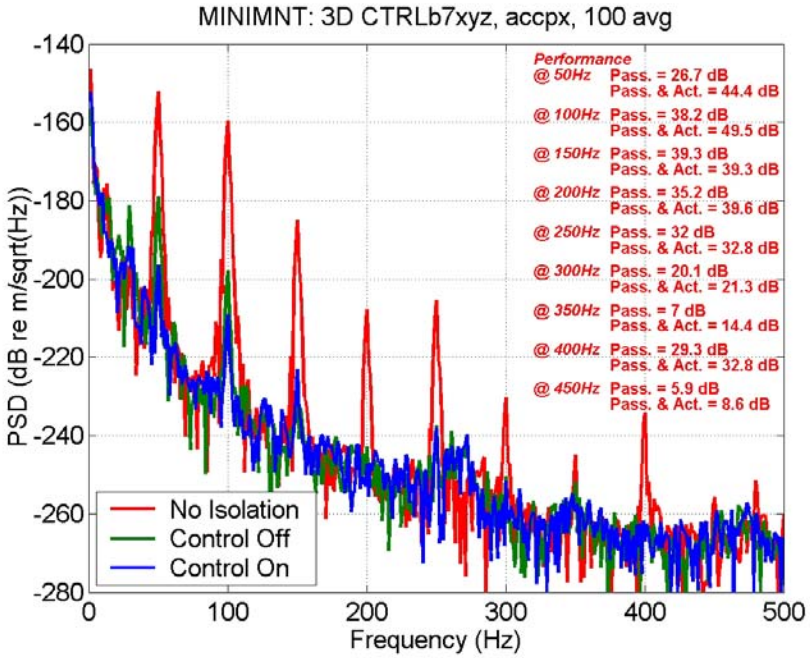

Fig. D4 — No-isolation/Control-off/Control-on frequency response display of **performance** accelerometer in **x-direction** due to multitone excitation.

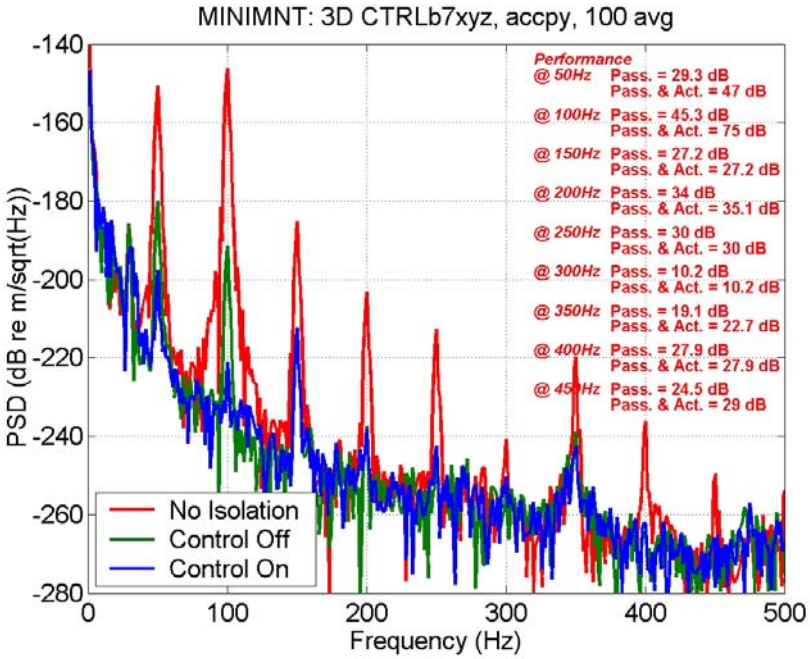

Fig. D5 — No-isolation/Control-off/Control-on frequency response display of **performance** accelerometer in **y-direction** due to multitone excitation.

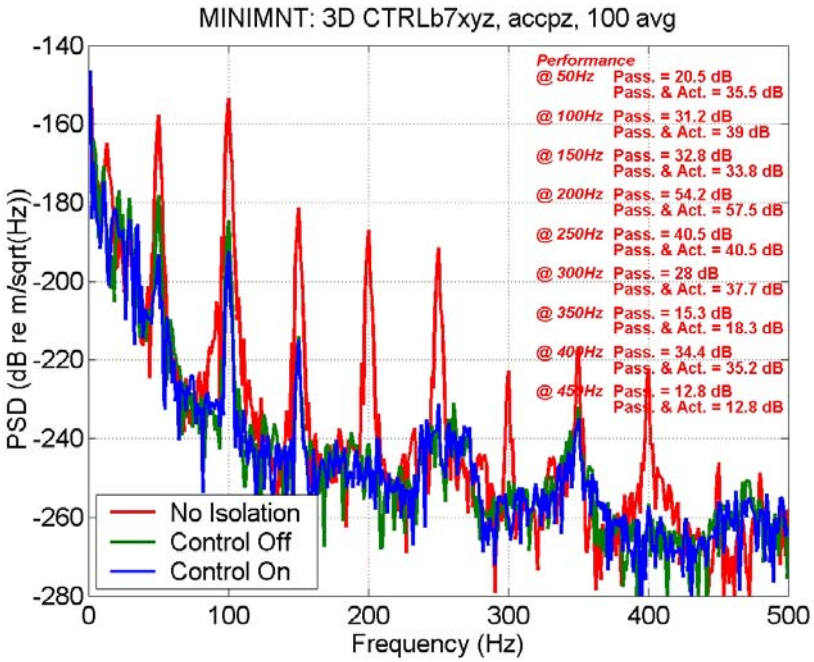

Fig. D6 — No-isolation/Control-off/Control-on frequency response display of **performance** accelerometer in **y-direction** due to multitone excitation.